PB83-191395

Validation of Samplers for Inhaled Particulate Matter

California Dept. of Health Services, Berkeley

Prepared for

Environmental Monitoring Systems Lab.
Research Triangle Park, NC

Mar 83

U.S. Department of Commerce
National Technical Information Service
NTIS

PB83-191395

EPA-600/4-83-010
March 1983

VALIDATION OF SAMPLERS FOR INHALED PARTICULATE MATTER

by

Walter John, Stephen M. Wall and Jerome J. Wesolowski
Air and Industrial Hygiene Laboratory
California Department of Health Services
Berkeley, California 94704

Final Report

Grant Number R806414-02

Ralph Baumgardner, Project Officer
Environmental Monitoring Systems Laboratory
U.S. Environmental Protection Agency
Research Triangle Park, North Carolina 27711

ENVIRONMENTAL MONITORING SYSTEMS LABORATORY
OFFICE OF RESEARCH AND DEVELOPMENT
U.S. ENVIRONMENTAL PROTECTION AGENCY
RESEARCH TRIANGLE PARK, NORTH CAROLINA 27711

REPRODUCED BY
NATIONAL TECHNICAL
INFORMATION SERVICE
U.S. DEPARTMENT OF COMMERCE
SPRINGFIELD, VA. 22161

TECHNICAL REPORT DATA
(Please read Instructions on the reverse before completing)

1. REPORT NO. EPA-600/4-83-010	2.
3. RECIPIENT'S ACCESSION NO. PB83 191395	
4. TITLE AND SUBTITLE Validation of Samplers for Inhaled Particulate Matter	5. REPORT DATE March 1983
	6. PERFORMING ORGANIZATION CODE
7. AUTHOR(S) Walter John, Steven M. Wall and Jerome J. Wesolowski	8. PERFORMING ORGANIZATION REPORT NO.
9. PERFORMING ORGANIZATION NAME AND ADDRESS Air and Industrial Hygiene Laboratory, California Department of Health Services, Berkeley, California 94704	10. PROGRAM ELEMENT NO.
	11. CONTRACT/GRANT NO. R806414-02
12. SPONSORING AGENCY NAME AND ADDRESS Environmental Monitoring Systems Laboratory Office of Research and Development U. S. Environmental Protection Agency Research Triangle Park, N. C. 27711	13. TYPE OF REPORT AND PERIOD COVERED FINAL - 11/78 to 11/81
	14. SPONSORING AGENCY CODE
15. SUPPLEMENTARY NOTES	

16. ABSTRACT Methods for the testing of new samplers for inhalable particles have been developed and applied to the dichotomous sampler and the size-selective hi-vol.

The sampling effectiveness of the inlet to the dichotomous sampler was measured and found to be excessively dependent on wind speed. A modification to improve the performance has been designed as a retrofit to the existing inlet. Wall losses in the dichotomous sampler were measured to be small. The fine fraction is found to be correlated to error in nozzle concentricity which is out of specifications in the typical commercial sampler.

Penetration of the size-selective hi-vol by solid particles larger than the 15 μm cutoff has been measured by three methods. Near the cutoff, monodisperse spray-dried particles, sized aerodynamically with a new Laser Sedimentation Velocimeter, were used. In the range 35-60 μm, glass beads and A/C test dust particles were produced by a new Sonic Fluidized Microbed Generator. Finally, ambient particles were analyzed by scanning electron microscopy on a Nuclepore after filter. All three tests show excess penetration of the size-selective hi-vol by solid particles to be acceptably small.

Additional testing was carried out in ambient air using an array of side-by-side samplers including two dichotomous samplers, two Monocut samplers and the AIHL cyclone.

KEY WORDS AND DOCUMENT ANALYSIS

17. a. DESCRIPTORS	b. IDENTIFIERS/OPEN ENDED TERMS	c. COSATI Field/Group

18. DISTRIBUTION STATEMENT Release to Public	19. SECURITY CLASS *(This Report)* Unclassified	21. NO. OF PAGES 89
	20. SECURITY CLASS *(This page)* Unclassified	22. PRICE

EPA Form 2220-1 (Rev. 4-77) PREVIOUS EDITION IS OBSOLETE

NOTICE

This document has been reviewed in accordance with U.S. Environmental Protection Agency policy and approved for publication. Mention of trade names or commercial products does not constitute endorsement or recommendation for use.

ABSTRACT

Methods for the testing of new samplers for inhalable particles have been developed and applied to the dichotomous sampler and the size-selective hi-vol.

The sampling effectiveness of the inlet to the dichotomous sampler was measured and found to be excessively dependent on wind speed. A modification to improve the performance has been designed as a retrofit to the existing inlet. The mechanical flow controllers for the dichotomous sampler are found to perform satisfactorily, but the Beckman rotameters and sample sealing system are found to be defective. Wall losses in the dichotomous sampler were measured to be small. The fine fraction is found to be correlated to error in nozzle concentricity which is out of specifications in the typical commercial sampler.

Penetration of the size-selective hi-vol by solid particles larger than the 15 μm cutoff has been measured by three methods. Near the cutoff, monodisperse spray-dried particles, sized aerodynamically with a new Laser Sedimentation Velocimeter, were used. In the range 35-60 μm, glass beads and A/C test dust particles were produced by a new Sonic Fluidized Microbed Generator. Finally, ambient particles were analyzed by scanning electron microscopy on a Nuclepore after filter. All three tests show excess penetration of the size-selective hi-vol by solid particles to be acceptably small.

Additional testing was carried out in ambient air using an array of side-by-side samplers. For the dichotomous sampler, the standard deviation of the coarse fraction concentration was more than twice that of the fine fraction. The fine fractions correlated closely with the mass concentration determined with the AIHL cyclone and the sum of the coarse and fine fractions correlated closely with the mass concentration from two Monocut inhalable particle samplers. One dichotomous sampler had a consistent bias of about -10% relative to the other samplers for undetermined reasons.

This report was submitted in fulfillment of Grant Number R806414-02 by the Air and Industrial Hygiene Laboratory, California Department of Health Services, under the sponsorship of the U.S. Environmental Protection Agency. This report covers the period November 1, 1978 to September 30, 1981, and work was completed as of November 20, 1981.

CONTENTS

Abstract iii
Figures v
Tables viii
Acknowledgement ix

1. Introduction 1
2. Conclusions 3
3. Recommendations 5
4. Methods for the Determination of the Particle Diameter of Monodisperse Test Aerosol 7
   Liquid Particles 7
   Solid Particles 8
5. Testing of the Dichotomous Sampler 11
   Inlet Testing 11
      Dimensions of Commercial Inlets for Dichotomous Sampler 11
      Sampling Effectiveness of the Inlets 14
      Development of Modified Inlets for the Dichotomous Sampler 14
   Flow Controller Performance and Calibration 21
   Impaction Stage Testing 26
      Dimensions of the Impaction Stages. 26
      Cutpoint and Wall Loss Measurements 30
6. Testing of the Size-Selective Hi-vol 43
   Dimensions 43
   Solid Particle Penetration Near the Cutoff 43
   Penetration by Large Particles. 48
      Sonic Fluidized Microbed Generator 52
      Large Particle Penetration Measurements 52
   Other Data on SSI Performance 62
   Large Ambient Particle Penetration 62
7. Side-by-Side Sampler Testing in Ambient Air 70

References 77

FIGURES

Number		Page
1	Inlets for the dichotomous virtual impactor	12
2	Experimental setup for static testing of inlets	15
3	Cutpoint of the inlet hat vs. the gap	16
4	Modified inlet including impactor A	18
5	Cutoff curve for impactor A alone	19
6	Cutoff curve for the modified inlet with impactor A	19
7	Cutoff curve for the inlet hat alone with a 6 cm gap	20
8	Comparison of measured cutoff to that calculated	20
9	Modified inlet with impactor B	22
10	Sampling effectiveness of impactor B alone	23
11	Flow meter calibration for coarse filter	24
12	Flow meter calibration for fine filter	24
13	Flow rate vs. pressure drop for fine filter	25
14	Flow rate vs. pressure drop for coarse filter	25
15	Casting method used for measurement of critical dimensions	27
16	Jig used for slicing nozzle replica	28
17	Experimental setup for simultaneous loading of five samplers	31

18	Coarse fraction vs. particle size for the dichotomous sampler	36
19	Total wall loss vs. particle size for the dichotomous sampler	36
20	Schematic drawing of impactor parts	37
21	Wall losses for individual parts of the dichotomous sampler	37
22	Total wall loss vs. error in nozzle concentricity	38
23	Fine fraction and wall loss vs. error in nozzle concentricity	39
24	Wall loss vs. fine fraction for DOP particles	41
25	Wall loss vs. mass loading	42
26	Size-selective hi-vol sampler	44
27	Key for dimensional measurements of the size-selective hi-vol	45
28	Experimental arrangement for measurement of penetration of the SSI by spray-dried solid particles	49
29	Location of 25 mm prefilter samplers inside the size-selective hi-vol	50
30	Sampling effectiveness of the SSI for liquid and solid particles	51
31	Schematic drawing of the Sonic Fluidized Microbed Generator	53
32	Detail of the base of the Sonic Fluidized Microbed Generator	54
33	Mean diameter of particles from the Sonic Fluidized Microbed Generator	54
34	Experimental arrangement for testing the SSI with the Sonic Fluidized Microbed Generator	56
35	Location of the fluidized bed, prefilter and after filter in the SSI	56
36	Photographs of the Sonic Fluidized Microbed Generator on the SSI	57

37 Size distributions of glass beads on the prefilter and after filter 59

38 Same as Figure 37 with larger glass beads 59

39 Photographs of glass bead deposits on the impaction plate of the SSI 60

40 Penetration of the SSI by large glass beads and A/C test dust 61

41 Sampling effectiveness of the SSI vs. flow rate 61

42 Correlation between entering concentration and filter deposit concentration 64

43 Correlation coefficients for various particle diameters 64

44 Arrangement for testing of the SSI with ambient particles 65

45 (a) Soil particles on prefilter, (b) XRF spectra 67

46 Size distribution of ambient particles on the prefilter and after filter 68

47 Coefficient of variation vs. concentration for the coarse fractions 72

48 Coefficient of variation vs. concentration for the fine fractions 72

49 Coefficient of variation vs. the sum of the fine and coarse fractions 73

50 Coefficient of variation vs. concentration for two Monocut samplers 73

51 Correlation between the concentration from Monocut samplers and the sum of fine and coarse fractions 76

52 Correlation between the fine fraction and the AIHL cyclone 76

TABLES

Number		Page
1	Flattening factors for DOP aerosol collected on 3M FC 721	9
2	Aerodynamic diameters from particle settling velocities	10
3	Dimensions of commercial dichotomous inlets	13
4	Critical dimensions of virtual impactors measured on replicas	29
5	Coarse fraction, fine fraction and wall loss of DOP particles in dichotomous samplers	33
6	Dimensions of the SSI tested in the present work	46
7	Sizes of glass beads and aerosol generated	55
8	Uniformity of filter deposits in the SSI	63
9	Penetration of the size-selective hi-vol by large ambient particles	69
10	Standard deviations and ratios of ambient particle concentrations from simultaneous operation of side-by-side samplers	74

ACKNOWLEDGMENTS

We thank Ralph Baumgardner, project officer, for his continuing interest and assistance. Daniel Rodgers participated in the experimental work.

SECTION 1

INTRODUCTION

The projects summarized in this report were undertaken to assist the Environmental Protection Agency in the development and validation of samplers for inhalable particulate matter. The samplers may be required for a new standard for particulate matter in ambient air being prepared by the EPA. The rationale for a standard for inhalable particles, those particles smaller than 15 μm aerodynamic diameter*, which are deposited in the respiratory system below the trachea, has been presented by Miller, et al. (1).

A trial network of inhalable particle samplers has been deployed across the nation by the Environmental Monitoring Systems Laboratory at Research Triangle Park, North Carolina (EMSL/RTP) in order to field test the sampling methodology and to acquire a data base in support of the new standard (2). Early results have revealed a number of technical problems with the samplers. For example, excessive differences are found between the particulate masses collected with side-by-side dichotomous samplers and there is a systematic difference in the mass concentrations measured by dichotomous samplers and size-selective hi-vols (2). Additional deficiencies have been discovered in laboratory testing, including a strong dependence on wind speed of the inlet to the dichotomous sampler (3). These experiences emphasize the need for rigorous testing of the new samplers, which will generate data upon which important control decisions will be based.

During the present project, laboratory tests were made on the dichotomous sampler and the size-selective hi-vol. Additional testing was carried out with side-by-side samplers in ambient air. New testing methods were developed, including measurement of nozzle alignment in the dichotomous sampler, precision wall loss measurements and tests for particle bounce. These test methods should be useful for the formulation of acceptance criteria for new candidate samplers and for quality assurance testing of commercial samplers.

*After the present work was completed, the EPA recommended a cutpoint of 10 μm for the revised particulate standard. Modified versions of the 15 μm samplers are now available. Some, but not all, of the test results presented here are outdated, but the test methodology is still current.

The present work was carried out in close cooperation with the EMSL staff and with other EPA contractors. For example, our work (in collaboration with J. Wedding, Colorado State University) uncovered the wind dependence of the dichotomous inlet (3). Subsequently, we participated in workshops at Research Triangle Park to develop criteria for a suitable inlet (4). Several groups then undertook the development of new inlets. Our contribution was the development of a modification enabling the retrofit of existing inlets.

SECTION 2

CONCLUSIONS

Inlets to commercial dichotomous samplers are found to adhere closely to manufacturing tolerances. However, wind tunnel and static chamber tests reveal excessive dependence of the sampling effectiveness upon wind speed. Flow visualization studies show strong channeling of the flow inside the inlet. A theoretical model including inertial and gravitational forces accounts well for the data. This provides a basis for a modification to the inlet consisting of an enlarged entrance slit and an inertial impactor. Tests of two versions show this to be a promising approach permitting a low-cost retrofit to existing inlets. The design facilitates a change in particle size cutpoint, should that be desired.

The mechanical flow controllers for the Sierra dichotomous samplers are found to perform satisfactorily. The Sierra samplers have an accurate flow calibration, but the Beckman rotameters are unreadable because of flow instabilities. In addition, the Beckman automatic sample changer does not seal the filter securely and there are leaks in the pumping system.

Measurements of the cutoff (coarse fraction vs. particle diameter) for the virtual impaction stage of the dichotomous sampler were made with DOP-uranine aerosol. Results were in excellent agreement with independent measurements by Loo and by McFarland. Measurements of the effectiveness of the hi-vol size-selective inlet made with DOP-uranine were also in good agreement with measurements made by Wedding in a wind tunnel at 2 km/hr and similarly by McFarland and Ortiz. These data show that independent laboratories can obtain consistent results for cutoff and effectiveness measurements using liquid aerosols.

A casting method was developed for the measurement of the critical dimensions of the dichotomous sampler stage. The nozzle concentricity was out of tolerance in 3 out of 5 samplers. Design faults are pointed out and a simple method suggested for improvement of the concentricity.

Laboratory tests with monodisperse aerosol show the 50% particle size cutpoint of the impactor stage of the dichotomous samplers to average 2.4 μm and the wall loss at the cutpoint to average 2.3%, both acceptable figures. Wall losses peaked at the cutpoint and increased again above 10 μm. The losses were mainly on the collection nozzle. While the wall losses were small for 3 μm particles, the fine fraction correlated with error in nozzle concentricity, making it desirable to hold the tolerance on the nozzle

concentricity. The magnitude of the wall loss was in agreement with the measurements by B. Loo and in disagreement with the results of A. McFarland. The losses at 2.5 μm are about twice as large as reported by Loo for the prototype. This is probably due to larger tolerances in the commercial versions for nozzle concentricity and collection nozzle profile. However, the wall losses are quite acceptable in the commercial units. The high precision of the present measurements obtained with standard laboratory equipment indicate that the present methodology affords a basis for a standard approach to sampler wall loss measurements.

Three methods have been developed for the measurement of the penetration of a size-selective sampler by large solid particles: (1) Near the cutoff, monodisperse spray-dried particles are used from a vibrating orifice aerosol generator and sized aerodynamically with a Laser Sedimentation Velocimeter. (2) Particles much larger than the cutoff are produced by a new Sonic Fluidized Microbed Generator from presized samples of glass beads and A/C Test (Arizona Road) Dust. (3) Penetration by large ambient particles is measured by microscopy on a Nuclepore after filter.

Method (1) could be applied directly to wind tunnel testing; however, since exposure to the aerosol material is difficult to avoid in wind tunnel work, it would be desireable to find a replacement for potassium biphthalate, which might be toxic. Method (2) cannot be applied in a wind tunnel without scaling up the output of the Sonic Fluidized Microbed Generator.

Applied to the Size-Selective Hi-vol, method (1) indicated 25% excess penetration by solid vs liquid particles at the 15 μm cutpoint. However, this would not ordinarily lead to a serious error in sampled mass since the cutpoint for solid particles is only slightly larger (17 μm) and the test particles are bouncier than most ambient particles. Method (2) shows 3-4% penetration by mass of glass beads and A/C Test Dust in the range of 35-60 μm aerodynamic diameter. 62 μm A/C Test Dust particles had 7% penetration, but this may be due to breakup of the particles, an inherent problem with A/C Test Dust. Glass beads were found to be an excellent test particle. Examination of the impaction plate showed that the particles did not adhere to the plate in the impaction zone but were collected near the bases of the collection tubes. Therefore the particles bounced, but were not reentrained in the exit flow. Method (3) gave a penetration efficiency of 5% for ambient particles greater than 30 μm aerodynamic diameter, in good agreement with method (2).

Ambient air testing with side-by-side samplers shows the standard deviation of the coarse fraction of the dichotomous sampler to be more than twice that of the fine fraction and nearly twice that of the Monocut samplers. The fine fractions correlated closely with the mass concentration from the AIHL (Air and Industrial Hygiene Laboratory) cyclone and the sum of the coarse and fine fractions correlated closely with the mass concentration from two Monocut inhalable particle samplers. One dichotomous sampler had a consistent bias of about -10% relative to the other samplers for undetermined reasons.

SECTION 3

RECOMMENDATIONS

The experience from the present program of validation of samplers for inhalable particles underlines the importance of rigorous testing. Precise tests with laboratory aerosol can lead to correction of problems before costly tests in ambient air. Sampler inlets need to be wind tunnel-tested to verify that wind speed sensitivity is within acceptable limits. Low wind speeds ($\tilde{<}$ 2 km/hr) should be included to ensure that particle sedimentation within the inlet is not significant. Testing should be done with monodisperse liquid particles for efficiency and wall loss measurements and with solid particles to determine possible excess penetration due to bounce and reentrainment.

During the present work several testing techniques were developed which are recommended for future work. The method for wall loss measurements is capable of accuracies approaching 0.1% and requires only standard apparatus. Three methods for measurement of solid particle penetration have been developed:

(1) Use of spray-dried particles from a vibrating orifice generator coupled with measurement of aerodynamic diameter with a Laser Sedimentation Velocimeter.

(2) Generation of large particles by a Sonic Fluidized Microbed Generator using presized glass beads.

(3) Microscopy of ambient particles on a Nuclepore after filter.

Additional work is needed for adaptation of (1) or (2) for wind tunnel measurements. For testing of an impaction stage in a sampler, static sampling is sufficient. The use of A/C Test (Arizona Road) Dust is not recommended due to its friable nature.

Testing with collocated samplers in ambient air has the potential to reveal additional "real world" problems. To identify the causes of the problems requires intensive hands-on work by research personnel. The present effort has involved an increasing number of samplers and auxiliary instrumentation. Operation of this array should be continued in an effort to reduce the coefficient of variation of concentrations measured with dichotomous samplers and to investigate the systematic difference in results from dichotomous samplers and size-selective hi-vols. New candidate samplers should also be tested in this manner.

The following specific recommendations are based on the present results:

(1) The inlet to the dichotomous sampler should be replaced with one which is insensitive to wind speed.

(2) Accurate nozzle alignment in the commercial dichotomous samplers should be ensured by the simple design change identified in the present work.

(3) The flow rotameters in the Beckman dichotomous sampler need to be stabilized and the sample changer mechanism redesigned to improve the sealing action.

(4) The Size-Selective Hi-vol has performed well under all testing thus far, justifying continued consideration as a candidate sampler.

SECTION 4

METHODS FOR THE DETERMINATION OF THE PARTICLE DIAMETER OF MONODISPERSE TEST AEROSOL

LIQUID PARTICLES

Currently, most laboratory testing and calibration of samplers is done with dioctyl phthalate (DOP) or oleic acid particles in the size range 0.5 to 20 μm. We have developed a reliable method for the sizing of these particles based on the calculation of the size from the operating parameters of the Berglund-Liu vibrating orifice aerosol generator (5) supplemented by continuous real-time measurements with a Climet optical particle counter.

While the calculated size has been found to be quite accurate, total reliance on it is inadequate because the Berglund-Liu generator is susceptible to malfunctions such as satellite generation, excessive coagulation into doublets, small particle size because of a very small syringe pump leak, etc. Some experimenters check the aerosol at the beginning of a run by taking a sample and examining it under a microscope. This is unsatisfactory since the number of particles sized is seldom sufficient for an accurate check, in fact, frequently only a visual inspection is made. Furthermore, conditions may change later during the run.

In our technique, a mother solution is made and diluted into a series of solutions for various particle sizes. These are successively run in the generator, monitored with the optical counter, and the peak channel determined in a multi-channel analyzer. The peaks corresponding to doublets, triplets, etc. are also recorded since these sizes are accurately known relative to the singlet. The resulting calibration curve is a smooth line on a log-log plot with a slope of 2.0 from 2.0 μm to 15 μm. The curve can be used to check subsequent sampler calibration runs which may take place over weeks of time, and to check dilutions for other particle sizes. During the runs, a portion of the aerosol is continuously sampled by an optical counter and the counter pulses and accumulated size distribution are displayed.

Periodically, an independent check of the particle size is made by collecting aerosol on a glass slide for microscope examination. The slide is treated with a hydrophobic fluorocarbon (3M Co. #FC 721, available from William F. Nye, Inc., New Bedford, MA, as Nyebar Type CT, 0.1%.) to inhibit particle flattening due to spreading on the surface. Slides are dipped in the solution and baked dry at 100°C. The diameters of collected particles are determined using a traveling hairline eyepiece (Nikon model EPOI 74 016). The

apparent particle diameter is multiplied by a flattening factor determined for this slide coating to yield the (spherical) geometric diameter. Flattening factors measured in our laboratory for DOP are listed in Table 1. For 10 to 20 μm particles, the flattening factor was very reproducible and insensitive to particle size.

SOLID PARTICLES

Laboratory measurements of particle bounce in air samplers often use spray-dried solid particles such as potassium biphthalate (KHP). In our laboratory KHP aerosol is generated and the particle size monitored with an optical particle counter in much the same way as for liquid particles. However, unlike liquid particles, the aerodynamic diameter for solid spray-dried particles cannot be directly calculated from operating parameters of the vibrating orifice generator, due to uncertainties in particle density and surface roughness. In order to measure aerodynamic diameter directly for these particles, the Laser Settling Velocimeter (LSV) was developed. The LSV consists of a vertical settling tube 0.7 cm I.D. illuminated from the bottom by a 5 mW He-Ne laser. The tube I.D. is critical; it has been determined empirically to minimize secondary air flow effects (private communication from D. Bright, National Bureau of Standards). A particle enters the top of the tube through a camera shutter which is then closed to isolate the air column from external air currents during the measurement. The settling velocity is measured for a single particle falling near the center line of the tube by recording the transit time between accurately spaced 10 cm divisions. The 5 mW laser provides sufficient illumination to visually observe particles larger than 10 μm. Aerodynamic diameters calculated from settling velocity measurements for dioctyl phthalate particles are shown in Table 2. The standard deviation of the settling velocity is based on the data of only about six particles, because of the high monodispersity of the aerosol and the high precision of the measurements. The results for these liquid particles agree very closely with aerodynamic diameters determined from the vibrating orifice generator parameters. The LSV was used to size all solid KHP aerosols used in this study.

TABLE 1. FLATTENING FACTORS FOR DOP AEROSOL[a] COLLECTED ON 3M FC 721

Geometric[b] Diameter (μm)	Collected[c] Diameter (μm)	Flattening[d] factor
10.0	13.4 ± 0.2	0.746
15.0	20.3 ± 0.2	0.739
18.0	24.2 ± 0.3	0.744
20.0	26.9 ± 1.0	0.743

[a]Contained 1% uranine by volume.

[b]Calculated from vibrating orifice generator operating conditions

[c]Aerosol collected on glass slide coated with 3M Company fluorocarbon #FC 721 and sized under optical microscope at 320 X using Nikon traveling hair line eyepiece.

[d]$$\text{Flattening factor} = \frac{\text{Geometric diameter}}{\text{Collected diameter}}$$

TABLE 2. AERODYNAMIC DIAMETERS DETERMINED FROM PARTICLE SETTLING VELOCITIES (Particles of Dioctyl Phthalate, 1% Uranine by Volume)

Calculated[a] Aerodynamic Diameter (μm)	Measured[b] Aerodynamic Diameter (μm)
9.97	9.99 ± 0.03
12.97	13.00 ± 0.06
14.96	14.97 ± 0.03
17.95	17.97 ± 0.09
19.95	19.96 ± 0.06

[a]Aerodynamic diameter calculated from operating parameters of vibrating orifice generator.

[b]Measurements made with Laser Settling Velocimeter.

SECTION 5

TESTING OF THE DICHOTOMOUS SAMPLER

The dichotomous sampler was one of the first particle samplers developed by the EPA as a replacement for the hi-vol (6,7,8). The dichotomous sampler provides two particle size cuts, an inhalable particle cutoff at 15 μm determined by the inlet, and a respirable particle cutoff at 2.5 μm produced by a virtual impactor stage. The present testing entailed:

(1) Determination of the wind dependence of the sampling effectiveness of the inlet; this important performance characteristic was not previously investigated for the commercial versions of the inlet.

(2) Development of a modification to the inlet to improve its sampling characteristics, since the commercial inlet was found to be deficient.

(3) A precision measurement of the wall losses in the dichotomous sampler to resolve a disagreement between two previous measurements (9,10).

(4) Correlation of the wall losses to dimensional parameters as a guide to quality assurance in sampler manufacture.

(5) Investigation of the performance and calibration of the flow controller.

INLET TESTING

Dimensions of Commercial Inlets for Dichotomous Samplers

The inlets studied were the Sierra Model 244, Model 244E (Sierra Instruments, Inc., Carmel Valley, California) and the Beckman (Beckman Instruments, Fullerton, California) which are commercial adaptations of the inlet designed by Wedding, et al. (11) (Figure 1). To check quality control and to compare different models, the dimensions were measured. The data listed in Table 3, show that replicate inlets of the same model are nearly identical. The principal differences between models are the presence of rain grooves in the Beckman inlet and Sierra's use of standoffs to support the inlet top, whereas the top of the Beckman inlet rests on the center tube. The center tube of the Sierra Model 244 does

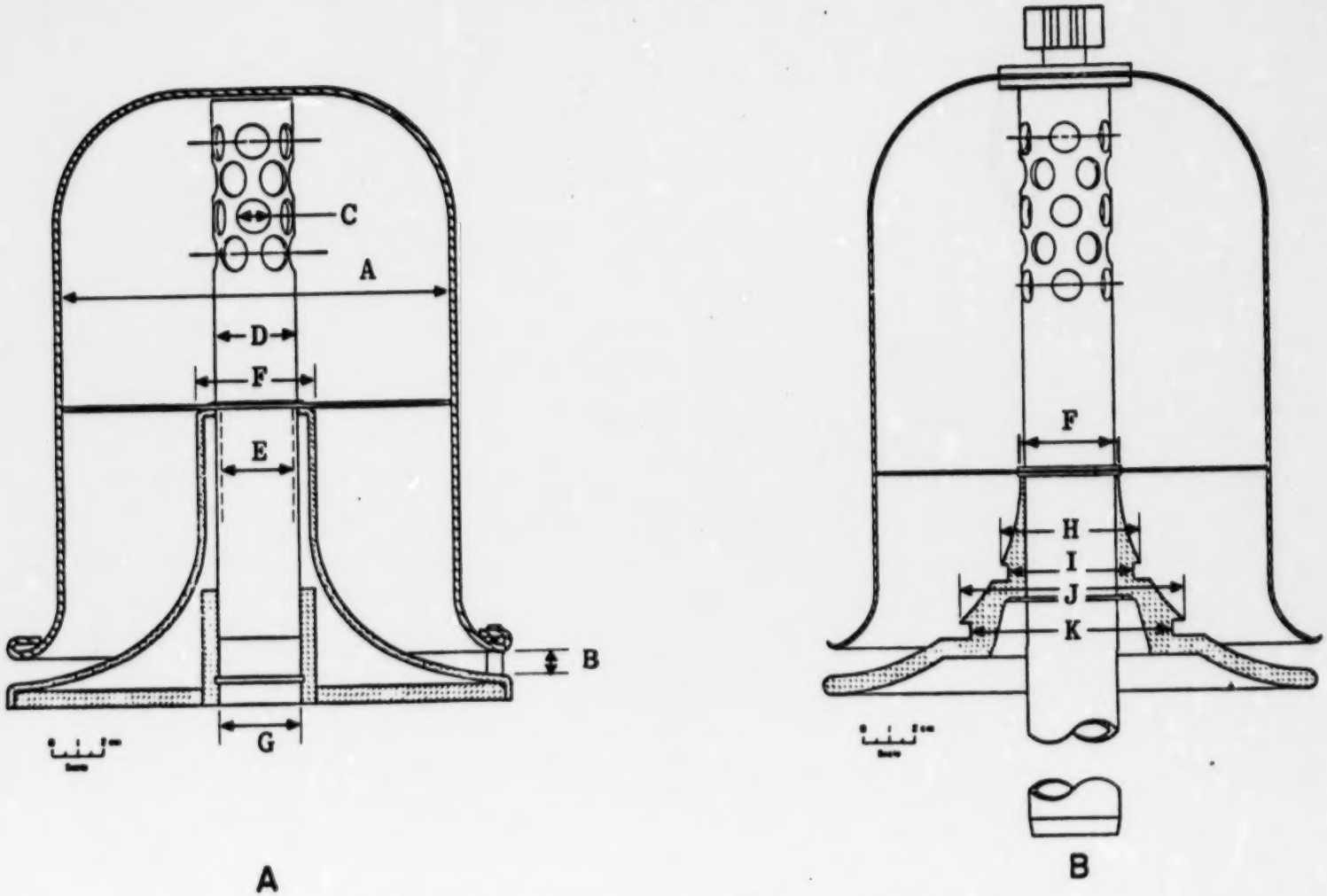

Figure 1. Inlets for the dichotomous sampler (a) Sierra Model 244E
(b) Beckman Automated Dichotomous Particulate Sampling System.

TABLE 3. DIMENSIONS (cm.) OF COMMERCIAL DICHOTOMOUS INLETS
KEY TO LOCATIONS IS GIVEN IN FIGURE 1

	Sierra 244 E		Sierra 244		Beckman	
Location	#2	#3	#149	#186	#036	#038
A	15.306	15.329	15.281	15.291	15.255	15.232
B	0.988	0.987	0.998	1.266	0.981	0.982
C	1.240	1.260	NA	NA	1.101	1.095
D	3.177	3.175	3.177	3.178	3.486	3.486
E	2.843	2.840	2.835	2.832	2.834	2.852
F	4.627	4.625	4.446	4.447	3.816	3.816
G	3.170	3.170	3.168	3.173	NA	NA
H	NA	NA	NA	NA	5.311	5.336
I	NA	NA	NA	NA	4.915	4.915
J	NA	NA	NA	NA	8.571	8.595
K	NA	NA	NA	NA	7.826	7.816

not have holes, but stops short of the top. Since Model 244 has been discontinued, no additional testing was made on this inlet.

The only significant dimensional difference was found in the inlet gap (dimension B) for Sierra Model 244E, No. 186. Apparently the standoff spacers were incorrectly cut for this inlet. The gap spacing could affect performance. Dimension F is somewhat smaller for the Beckman inlets. For the most part, however, the manufacturing is found to adhere to close tolerances.

Sampling Effectiveness of the Inlets

Details of the tests and the results have been published by Wedding, et. al (3). The abstract is given below as a summary.

> "The sampling effectiveness of the inlet to the dichotomous virtual impactor has been measured in a wind tunnel at speeds from 5 to 40 km/hr using monodisperse oleic acid particles 5 to 30 μm aerodynamic diameter. A static test was performed at near-zero wind speed. Over this range of wind speeds the 50% cut point varied from 10 to 22 μm, with a maximum near 2.5 km/hr. At a given wind speed the cutoff curve (effectiveness vs. particle diameter) is not sharp. Flow visualization studies revealed strong channeling of the flow inside the inlet. A simple theoretical model based on this flow pattern including inertial and gravitational forces on the particles accounts well for the observations. It is concluded that a better inlet is required for the dichotomous sampler. The present experience indicates the need for rigorous experimental validation of new inlet designs."

Development of Modified Inlets for the Dichotomous Sampler

The inlet tests reported above showed excessive dependence of the sampling effectiveness on wind speed. Subsequent workshops held at Research Triangle Park established performance criteria for an inhalable particle inlet (4). Since the current inlet does not satisfy these criteria, it is necessary to equip the samplers with an improved inlet. One possibility, pursued here, is to modify the existing inlet to improve the performance. The intention is to provide a relatively simple, low cost retrofit. The modification presented below has the advantage of having a cut point which can be easily changed, if that should be desired.

The modification was based on our work on the original inlet in which a basic understanding of the physics was achieved. The first step was to increase the annular gap to break up the channeling of the flow. Figure 2 shows the test setup for measurements. Figure 3 is a graph of D_{50} vs. gap height. At 1 cm (the original gap) and at 2 cm there is very little change with height as our theory predicts. At still larger gaps the channeling becomes less pronounced and D_{50} increases. At about 3 cm, the area of the annular gap is about equal to the cross sectional area inside the hat (bell-shaped cover). Above 4 cm, the curve is leveling off; the gap is becoming a smaller factor in

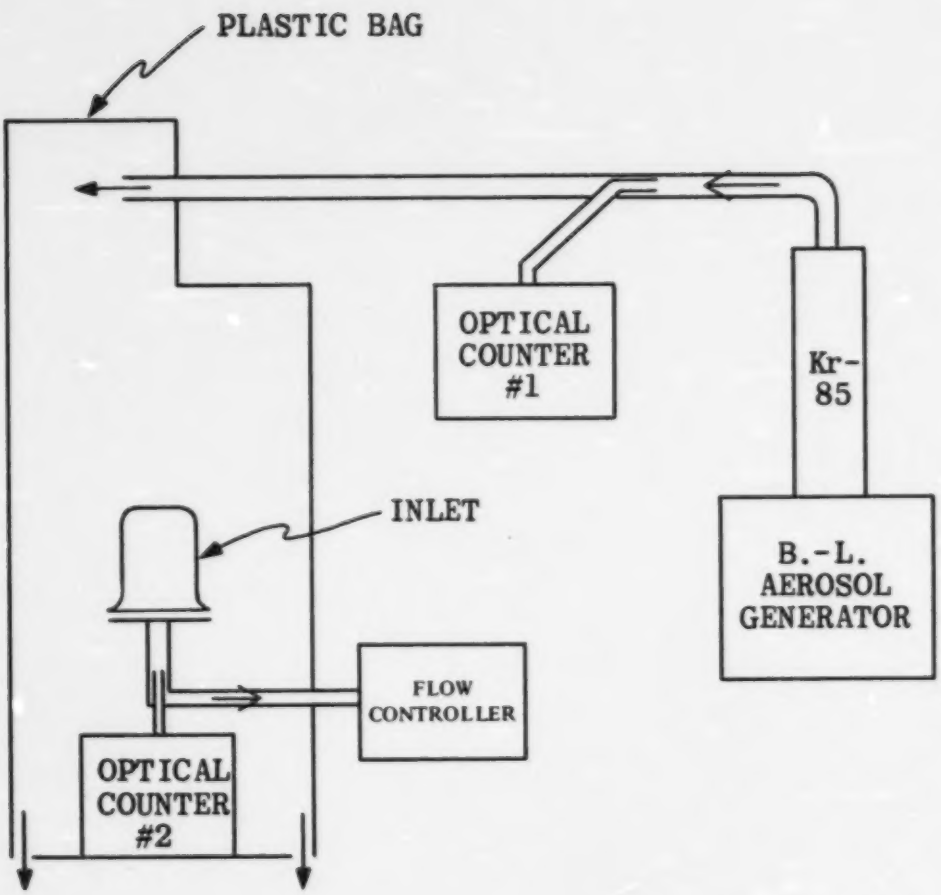

Figure 2. Experimental setup for static testing of inlets with monodisperse aerosol.

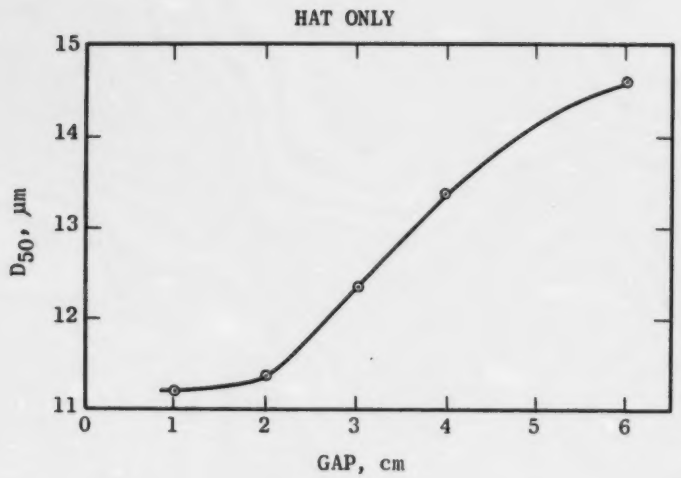

Figure 3. Cutpoint of the inlet hat vs. the gap (height of inlet slit).

determining D_{50}. We chose to use a gap of 6 cm, the minimum we can use at zero wind speed, in order to preserve the performance at higher wind speed.

Next, an inertial impactor was designed to provide a definite particle size cut. Two versions of this impactor were developed, designated impactors A and B. The impactor slips onto the central tube, which is shortened as shown in Figure 4. The impaction plate is porous sintered stainless steel saturated with a low vapor pressure oil which prevents particle bounce (12). The cutoff curve for impactor A alone is shown in Figure 5.

The solid particle data requires explanation. Initially, the size was determined as follows: from the Berglund Liu parameters the particle mass is known, and by optical microscopy, the geometric particle diameter is measured. The density ρ is then calculated. Then $D_{aerodynamic} = \rho D_{geom}$. We found that the solid particle points were about 1 µm smaller than indicated from the curve calibrated with oleic acid. Under the scanning electron microscope, we could see surface structure with void spaces. This surface structure evidently has a small effect on the aerodynamic drag. Hence we applied a correction factor to shift the solid particle points onto the curve, since solid and liquid particles should have the same efficiency on the oil-soaked plate. This correction factor, 1.06, was used throughout. The data still can be used to indicate the absence of bounce since bounce would change the shape of the curve, i.e., there would be increased penetration of solid particles at larger particle sizes.

In Figure 6, the complete AIHL inlet assembly is shown to have a cutoff of 13 µm. The solid points lie on the same curve.

Figure 7 is the cutoff for the hat only. We don't understand why the penetration of solid particles is somewhat lower than that for liquid particles at the larger sizes.

In Figure 8 we have calculated the cutoff of the assembly by multiplying hat only efficiency (oleic acid) by the impactor only efficiency. Good agreement is obtained with the measurements.

Preliminary tests in the wind tunnel at Colorado State were promising but the cutpoint dropped to 12.5 µm at 24 km/hr. (13 µm is within the EPA acceptance criteria.)

Impactor B was developed to improve the performance of the modified inlet at non-zero wind speeds. The outside diameter of the impactor was reduced in order to avoid imparting an outward radial component of velocity to the air moving upward inside the hat. The cutpoint of the impactor was increased to 20 µm so that the cutpoint of the inlet assembly would be closer to 15 µm. Tests of various impactor configurations were made with the experimental setup shown in Figure 2, the optical counter making it possible to obtain results within a few minutes.

At first an impactor similar to impactor A but with reduced outside diameter was tried. This was unsuccessful because of excessive wall losses caused by the reduced clearance around the impaction plate. A different

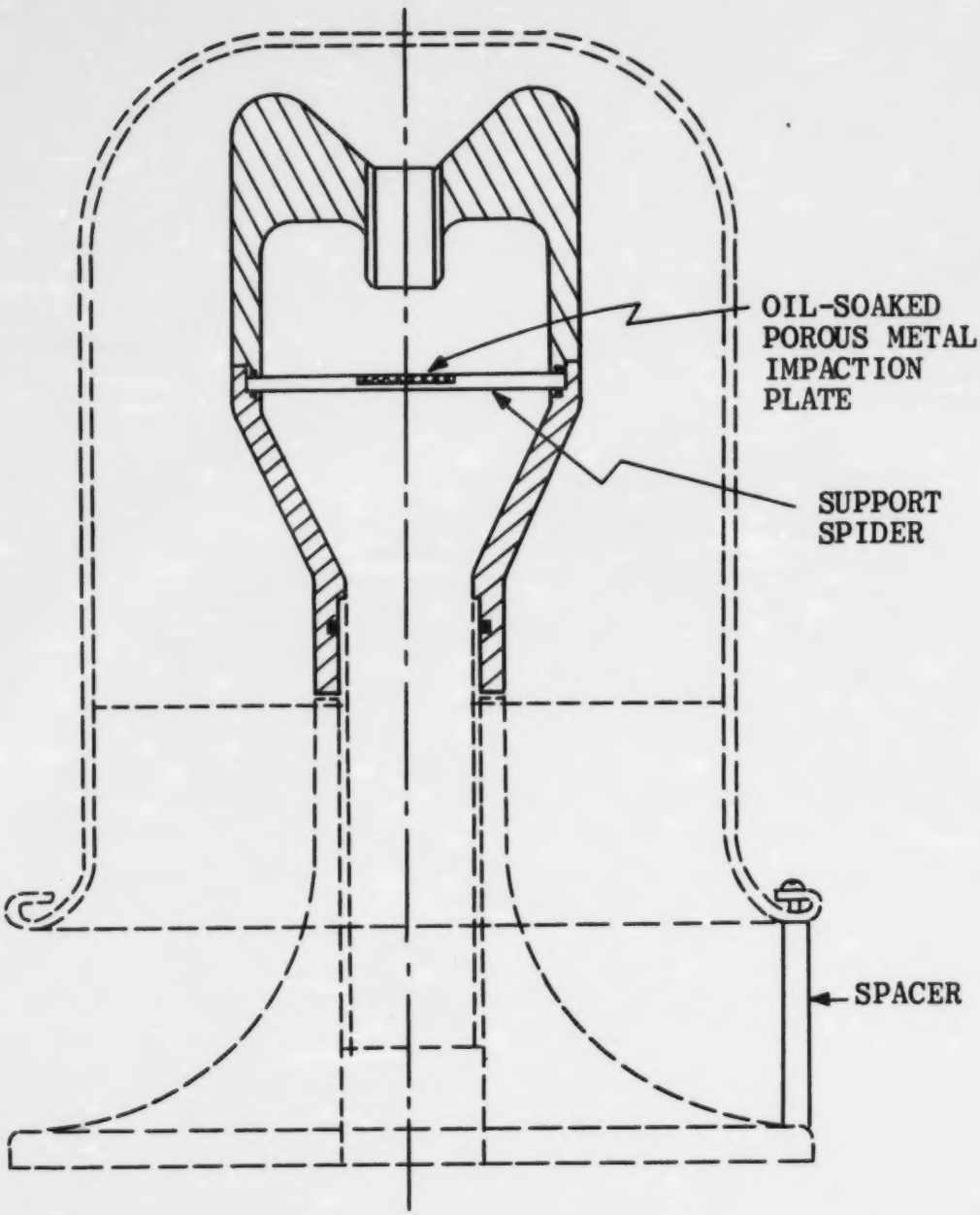

Figure 4. Modified inlet including impactor A to provide a definite cutpoint and a spacer to increase the gap. Original inlet parts are shown in dashed lines.

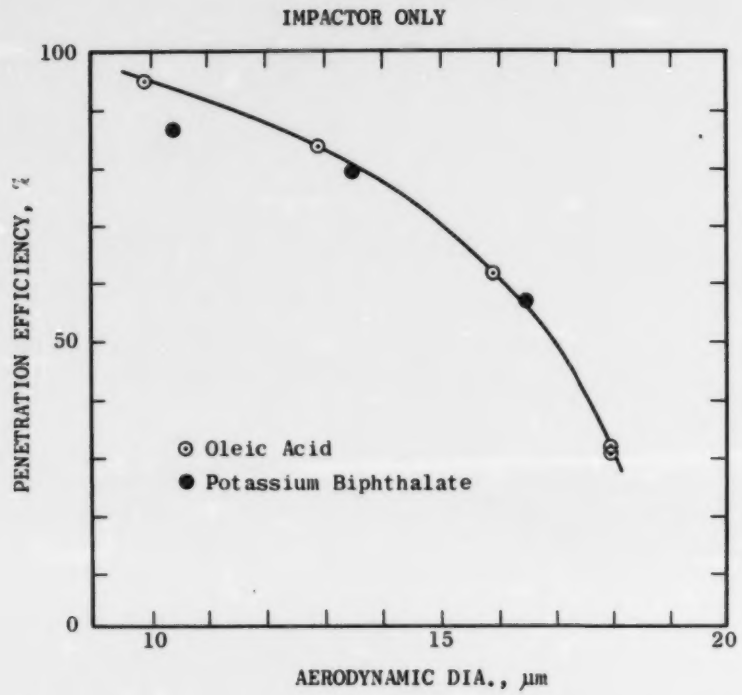

Figure 5. Cutoff curve for impactor A alone for liquid (oleic acid) and solid (potassium biphthalate) particles.

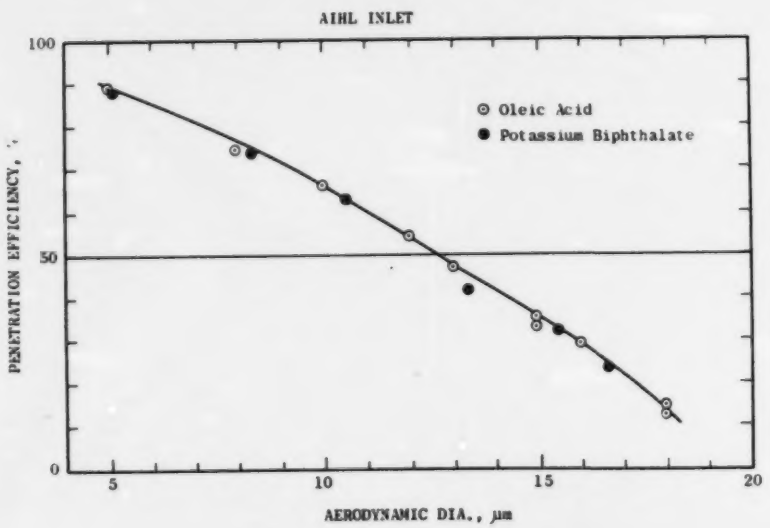

Figure 6. Cutoff curve for the modified inlet with impactor A at near-zero wind speed.

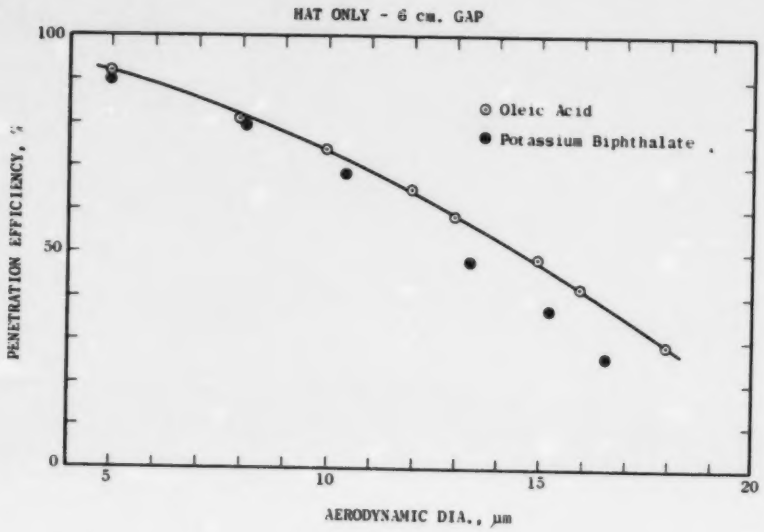

Figure 7. Cutoff curve for the inlet hat alone with a 6 cm. gap.

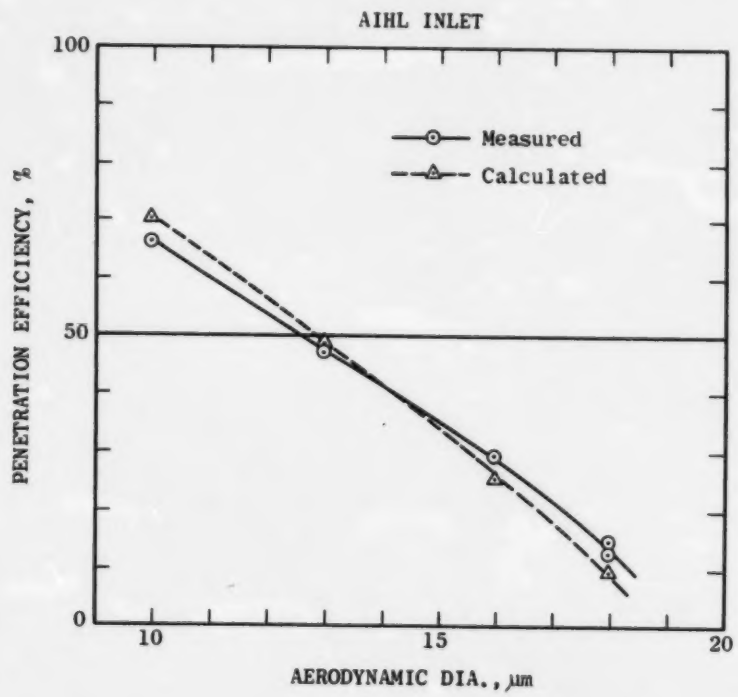

Figure 8. Comparison of measured cutoff to that calculated from impactor A alone and hat alone data.

approach was then tried which proved successful. The final version of impactor B is shown in Figure 9. The entire impactor is housed within a tube the same diameter as the upper base of the inlet. The air is accelerated through an annular slit, impinges on a porous metal impaction plate and then exits through a hole in the center. Since the flow is away from the wall, losses are not expected nor, indeed, observed. A number of variations on this basic configuration were tried; two aspects are worthy of mention. At first the piece forming the inner wall of the acceleration slit was held by a spider having three radial pins. The turbulence from the pins created three spots of enhanced deposition on the plate. These were eliminated by suspending the center part of the slit from the top, as shown in Figure 9. This also provides convenient access to the porous plate. Secondly, various lips were tried on the inner edge of the impaction plate, with varying center hole diameter, etc. All were found to degrade the sharpness of the cutoff.

The cut point was determined with liquid (oleic acid) and solid (potassium biphthalate) particles. Both fell on the same curve (Figure 10) with a 50% cut point at 20 μm. To date impactor B has not been tested in a wind tunnel.

A slightly scaled-down version of impactor B was recently tested by McKenzie, et al. (13) for use as an inlet for a small portable inhalable sampler. Their version, which is used without a hat, has a 15 μm cutpoint and has a cutoff satisfying the EPA criteria.

FLOW CONTROLLER PERFORMANCE AND CALIBRATION

The flowmeter in each control module was calibrated against a wet test meter (American Meter Company, DOH #32155). The wet test meter had previously been calibrated against a spirometer (American Meter Company, DOH #31616). To insure the validity of the measurements in the flow ranges of interest, the wet test meter was also compared to a dry test meter (American Meter Company, #ARB-358-004) and a manufacturer's calibrated rotameter (Gilmont Serial #556).

The pumping systems of the control modules were designed to maintain a constant flow rate as pressure is reduced by filter loading. To test this constancy of flow a needle valve was placed at the inlet to reduce the flow entering the unit. To test whether the flow rate measured by the instrument's flowmeter located near the outlet is the same as that entering the unit, a rotameter was attached upstream of the needle valve. A properly functioning control module will show the same flow rate, measured by the internal and external flowmeters, as the pressure is reduced by the needle valve to simulate filter loading. This flow rate should be constant up to a reasonable pressure drop. Pressure drop was measured by the vacuum gage in the control module.

Data for a Sierra 244 control module are shown in Figures 11 and 12. The flowmeters are found to be accurately calibrated. In Figure 13, the flow rate is shown to be constant until a pressure drop of about 15 in. Hg was reached, then the flow rate dropped rapidly. Also included on Figure 13 is the change in total flow as pressure is lowered. This total flow rate vs. pressure curve

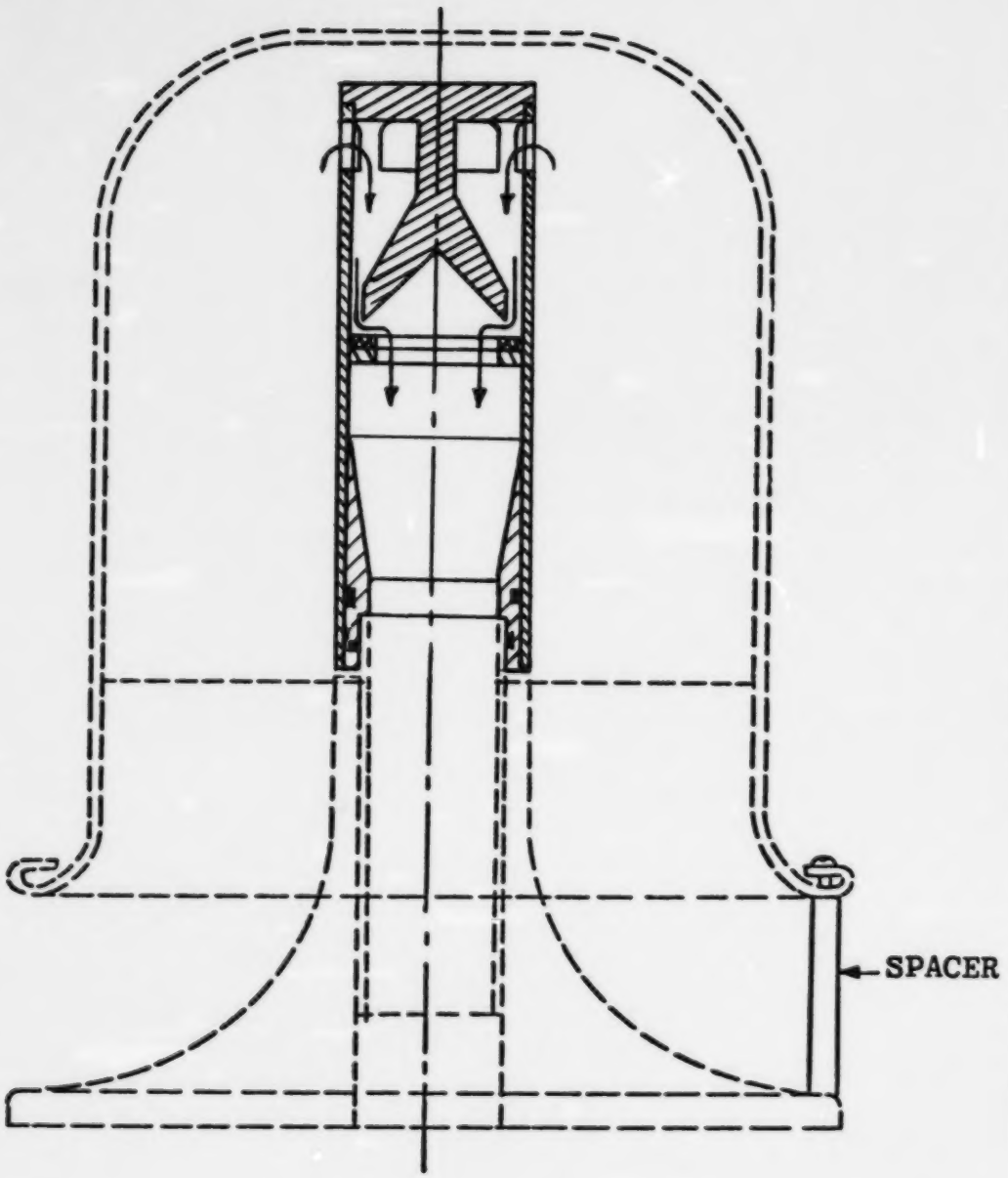

Figure 9. Modified inlet with impactor B. Original inlet parts are shown in dashed lines.

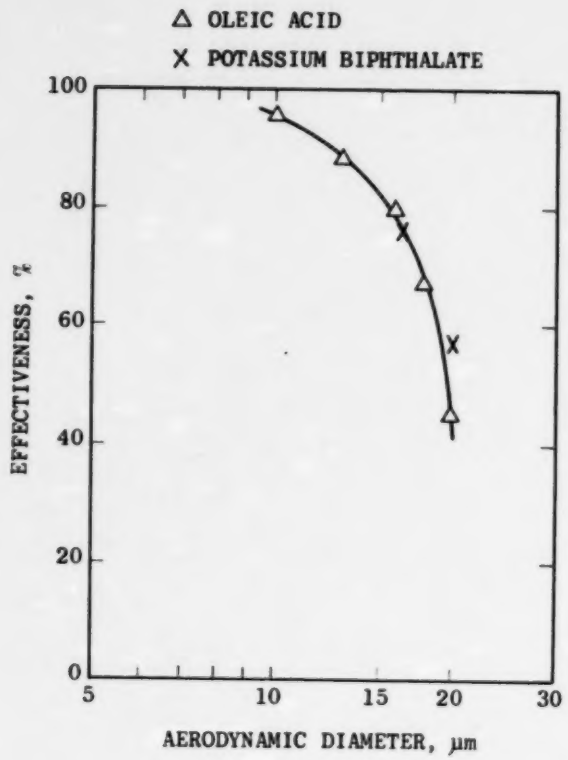

Figure 10. Sampling effectiveness of impactor B alone showing the same cutoff for both liquid and solid particles.

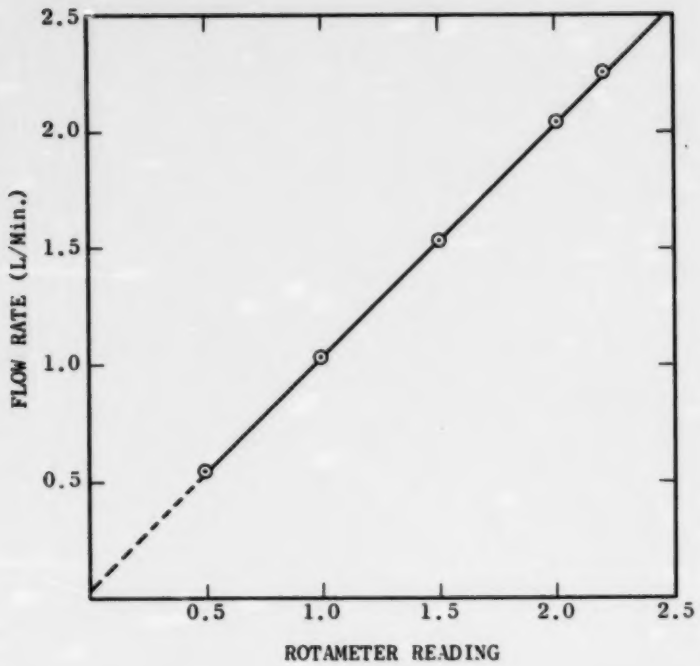

Figure 11. Flowmeter calibration curve for Sierra Model 244, coarse filter.

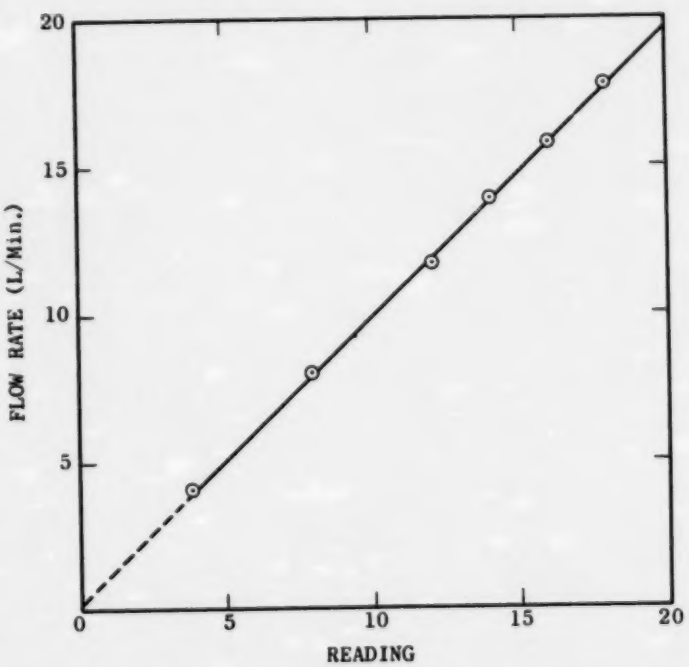

Figure 12. Flowmeter calibration curve for Sierra Model 244, fine filter.

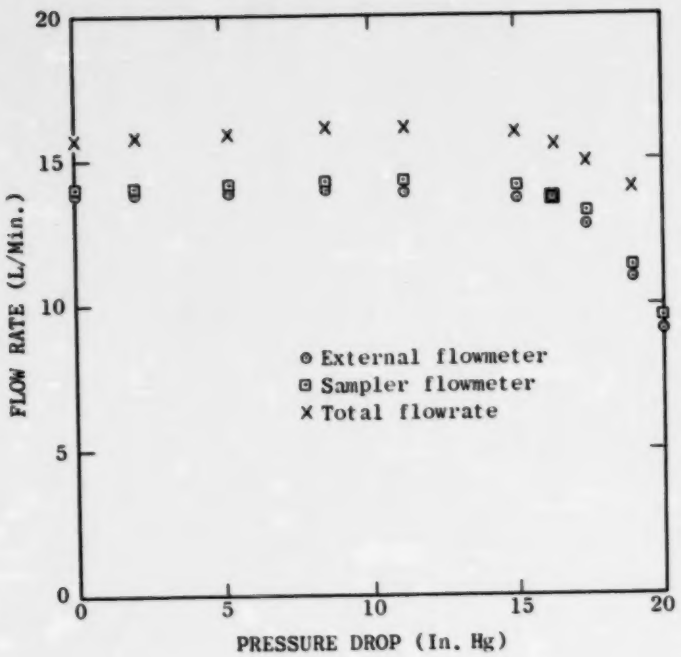

Figure 13. Flow rate vs. pressure drop for Sierra Model 244, fine filter.

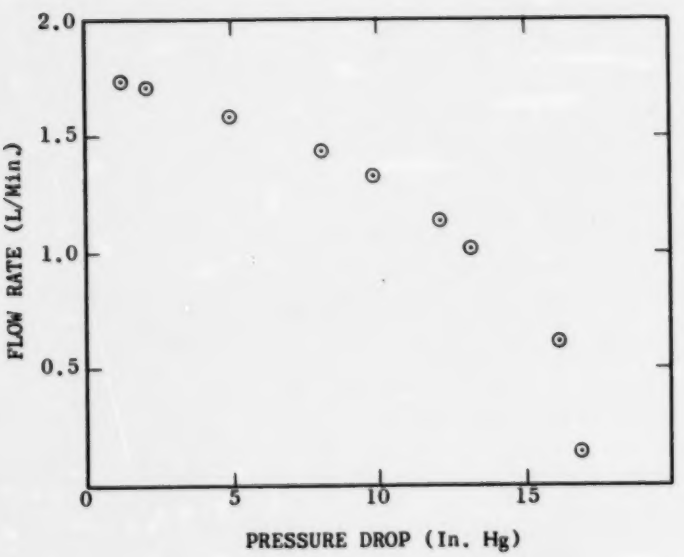

Figure 14. Flow rate vs. pressure drop for Sierra Model 244, coarse filter.

parallels the high flow rate curve. The lowering of pressure in the high flow system had no effect on the low flow rate. Both internal and external rotameters agreed.

Figure 14 shows the variation in flow rate in the low flow rate system vs. pressure drop. In this case the flow rate started to decrease as soon as pressure was lowered and steadily decreased until the flow was zero. The total flow rate remained constant throughout this experiment and the high flow rate increased slightly. Thus, the high flow rate increased by about the amount the low flow rate decreased keeping the total constant. This is expected for this type of single pump system with the total flow rate controlled by a diaphragm.

The performance of this Sierra control module was satisfactory. Tests of two additional units yielded very similar results. The Beckman flowmeters have been found to oscillate in such a manner as to prevent meaningful readings. A change in the apparatus will be necessary to eliminate the unstable flow at the rotameters.

IMPACTION STAGE TESTING

Dimensions of the Impaction Stages

Measurements of critical dimensions are necessary so that practical tolerances can be established in terms of performance. Critical dimensions include the inside diameters of the acceleration and collection nozzles, their concentricity, the internozzle distance and the contour of the collection nozzle.

Determination of the nozzle concentricity and spacing in the assembled unit is difficult with conventional machinist's gages. A new technique was therefore developed, using a dental impression material [Surgident Neo-Plex Rubber Base Impression Material (Regular Body) Cat. No. 56067, Lactona Co., Morris Plains, NJ 07950]. The material is injected into the assembled impactor through the acceleration nozzle (see Figure 15) and allowed to harden. The resultant impression is then sliced in half along the axis of the sampler in a special jig (Figure 16). The replica then exhibits the profile of the inside of the critical nozzle area. Measurements are made under a Zeiss microscope at 50X using a long working distance objective. The replica is translated by an X-Y stage with 0.002 mm (8 microinches) resolution.

A preliminary evaluation of the technique was made by comparing the result for the inside diameter of the collection nozzle from the replica to that from a direct mechanical measurement. The replica was found to be systematically 0.8% smaller. Subsequent measurements of hole diameters were corrected by 0.8%. Shrinkage of the casting was found to be $< 0.2\%$ after 1 month and $< 0.35\%$ after 6 months.

Measurements on three Sierra and two Beckman samplers are listed in Table 4. Data are given for replicas cut at azimuthal angles of 0, 45 and 90°

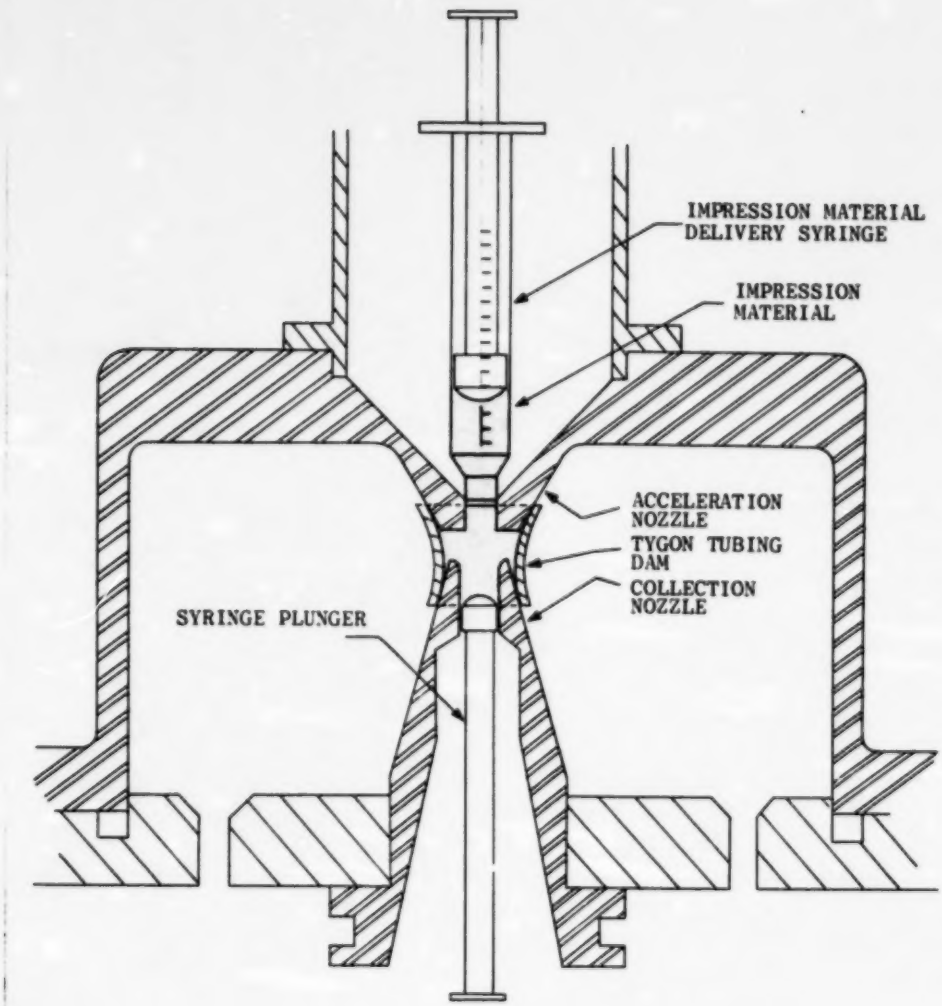

Figure 15. Casting method used to produce replicas for measurement of critical dimensions of the virtual impaction stage.

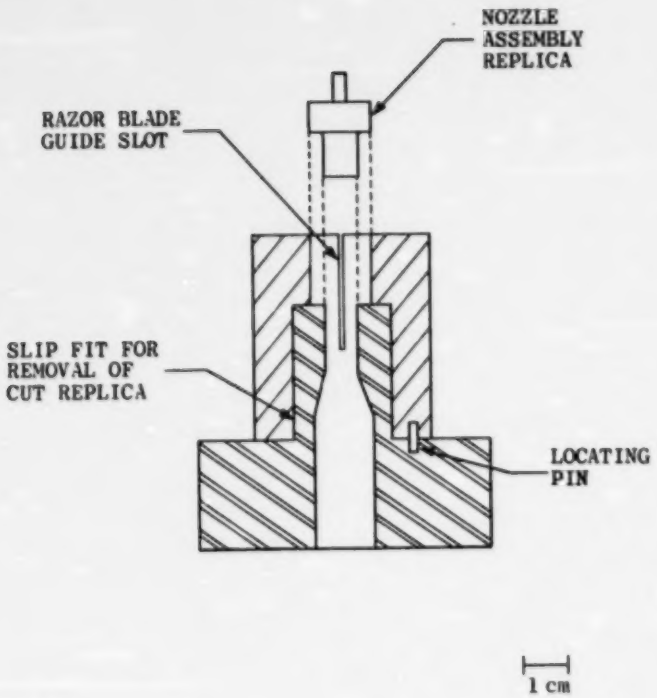

Figure 16. Jig used to hold the nozzle assembly replica for slicing in half.

TABLE 4. CRITICAL DIMENSIONS (INCHES) OF VIRTUAL IMPACTORS MEASURED ON REPLICAS

Model No.	cutting angle	inlet nozzle diameter	collection nozzle diameter	inter nozzle distance	error in nozzle concentricity
Sierra #186					
replica #1	0°	0.1194 ± 0.0003	0.1662 ± 0.0002	0.1284 ± 0.0002	0.0004 ± 0.0004
replica #6	45°	0.1195 ± 0.0001	0.1647 ± 0.0001	0.1299 ± 0.0001	0.0007 ± 0.0006
replica #5	90°	0.1188 ± 0.0002	0.1672 ± 0.0002	0.1279 ± 0.0003	0.0027 ± 0.0007
Sierra #149					
replica #1	0°	0.1198 ± 0.0001	0.1670 ± 0.0001	0.1300 ± 0.0004	0.0013 ± 0.0001
replica #2	45°	0.1201 ± 0.0001	0.1660 ± 0.0001	0.1299 ± 0.0003	0.0024 ± 0.0001
replica #3	90°	0.1203 ± 0.0001	0.1666 ± 0.0001	0.1296 ± 0.0002	0.0004 ± 0.0001
Sierra #151					
replica #5	0°	0.1196 ± 0.0002	0.1663 ± 0.0001	0.1295 ± 0.0004	0.0057 ± 0.0010
replica #2	45°	0.1195 ± 0.0003	0.1666 ± 0.0004	0.1293 ± 0.0004	0.0016 ± 0.0001
replica #7	90°	0.1199 ± 0.0002	0.1665 ± 0.0002	0.1318 ± 0.0004	0.0055 ± 0.0001
Beckman 038					
replica #1	0°	0.1206 ± 0.0001	0.1659 ± 0.0002	0.1264 ± 0.0006	0.0021 ± 0.0004
replica #7	0°	0.1207 ± 0.0000	0.1659 ± 0.0001	0.1265 ± 0.0001	0.0024 ± 0.0002
replica #2	45°	0.1206 ± 0.0001	0.1663 ± 0.0001	0.1256 ± 0.0003	0.0037 ± 0.0003
replica #10	90°	0.1212 ± 0.0001	0.1665 ± 0.0000	0.1263 ± 0.0001	0.0042 ± 0.0002
Beckman 036					
replica #9	0°	0.1205 ± 0.0002	0.1668 ± 0.0002	N/A	0.0010 ± 0.0001
replica #11	45°	0.1192 ± 0.0001	0.1666 ± 0.0001	0.1247 ± 0.0005	0.0016 ± 0.0003
replica #13	90°	0.1200 ± 0.0000	0.1669 ± 0.0001	0.1238 ± 0.0002	0.0010 ± 0.0005
Design Specifications		0.120 ± 0.005	0.166 ± 0.005	0.125 ± 0.005	$\leq$ 0.002

to check the concentricity. The triplicate measurements of the diameters and internozzle distances show the high precision of the technique.

All samplers were within specifications for inlet nozzle diameter, collection nozzle diameter and inter-nozzle distance. For nozzle concentricity, one sampler was within specification, two were close and two (a Beckman and a Sierra) were out of specification by more than twice the allowable tolerance.

In the Beckman sampler, the nozzles are mounted on circular flanges which are sealed to the inside of a cylinder by sliding O-rings. Thus the positioning of the nozzles is directly affected by variations in the compression of the O-rings. Also, the assembly consists of four pieces which must be accurately located relative to each other.

The Sierra nozzles are positioned by metal-to-metal contact but the assembly also consists of four pieces. We suggest that the accuracy could be improved by the following procedure: First, the pieces are assembled, but with undersized holes in the nozzles. Then the holes are reamed out to the correct diameter while the parts are assembled. The parts should be keyed or pinned so that they fit together in one orientation only. This procedure would greatly increase the accuracy of alignment at small additional cost. The replica also faithfully reproduced the profile of the tip of the collection nozzle. This was examined in the microscope and on enlargements of photomicrographs. Typically, the radius of the inner lip subtends an arc of less than 90°, so that the curved surface is not tangent to the flat surface. The cut is not deep enough and the resulting corners are not polished off. This is difficult to quantify, nor does it appear necessary, judging from the small measured particle losses reported below.

Cutpoint and Wall Loss Measurements

The experimental arrangement is shown schematically in Figure 17. Monodisperse dioctylphthalate (DOP) particles tagged with uranine are produced by a Berglund-Liu vibrating orifice aerosol generator and passed over a Kr-85 radioactive source for reduction of electrical charge. With the valve in the position shown, aerosol is conducted to a manifold via a horizontal brass pipe. Clean dilution air is introduced along the lower half of the pipe as shown. This effectively reduces particle losses by sedimentation, and is necessary in order to obtain usable concentrations of particles with diameters 15 μm or larger. A symmetrical pipe arrangement supplies aerosol to five samplers. This ensures that the samplers receive particles of identical size and nearly equal concentrations. A Climet 208 optical counter monitors the aerosol concentration and size distribution.

Before each run the valve above the Kr source was placed in the vertical position so that clean air only was supplied to the manifold. A calibrated rotameter was attached to each sampler inlet in turn to check the flow rate and the filter sealing. The Beckman samplers were found to have an unreliable sealing action. It was necessary to manually adjust the sealing mechanism until a satisfactory seal was achieved. There were two additional problems with both Beckman samplers. The pumps for the fine-fraction leaked and the

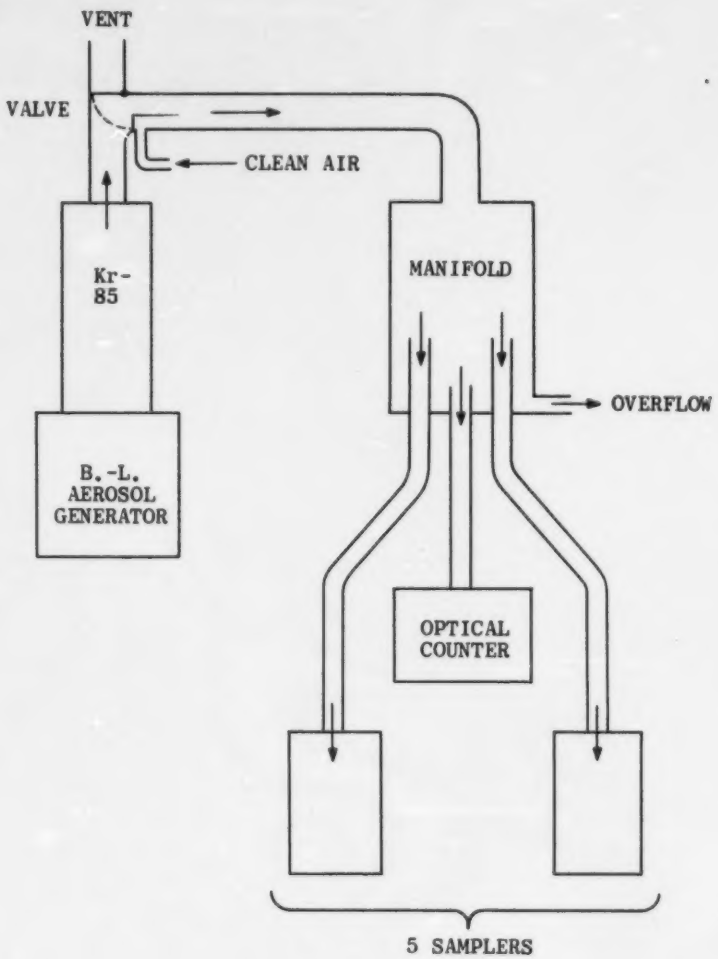

Figure 17. Experimental setup for simultaneously loading five samplers with monodisperse aerosol.

pulsation of the rotameters made them unreadable. Therefore, the fine fraction filter was pumped by an external Sierra flow controller for these tests.

The aerosol generator was turned on and the particle size and concentration allowed to approach steady values. The samplers were turned on with clean air only in order to avoid any transient, unrepresentative sampling losses. Then the valve was switched to supply aerosol and the run commenced. After the run the samplers were disassembled and the parts (see Figure 20) rinsed down separately with 90% isopropyl alcohol -- 10% water solution using a wash bottle. Only the inside surfaces were washed. The parts with the major deposition were washed twice and the washings quantitated separately. Recovery in the first wash was approximately 90%. The filters were placed in beakers, covered with solvent, and sonicated for 10 minutes. Repeated washings showed that the first washing recovered 99% of the deposit on the Teflon membrane filters.

Results are summarized in Table 5. For individual samplers, the standard deviations are computed from repeated trials. The standard deviations are also given for each sampler type. An analysis of variance applied to the raw data showed that there was no significant difference ($P > 0.8$) between the wall losses in the Sierra vs. the Beckman samplers.

In Figure 18, the coarse fraction averaged over all samplers is plotted against the aerodynamic particle diameter. The 50% cutpoint occurs at 2.4 μm. Good agreement is obtained with the results of Loo (9), and fair agreement with those of McFarland (10).

The total wall loss is shown as a function of particle diameter in Figure 19. The losses peak at the cutpoint and rise rapidly above 10 μm. Excellent agreement is obtained with the results of Loo (9), except at 2 μm. On the other hand, McFarland's (10) results are higher by a factor of 3 at 2.5 μm and a factor of 2 at 15 μm. The wall losses are plotted in Figure 21 by sampler part (labelled as in Figure 20). Near the 2.5 μm cutpoint, the losses are mainly on the collection nozzle. At 15 μm, the largest loss is still on the collection nozzle but losses increase in the acceleration nozzle. The loss in the drift tube (D) was significant only at 15 μm, appearing where the sudden increase in tube diameter occurs at the juncture of parts C and D. It was seen in some samplers and not in others. In Figure 22, the total wall loss for each sampler is plotted vs. the measured error in nozzle concentricity for particle diameters of 2.0 and 2.5 μm. The wall loss shows no particular dependence on the concentricity; moreover, since the maximum loss of 2.6% is well within acceptable limits, the manufacturing tolerances, although outside of specifications, are also acceptable.

For 3.0 μm particles, the wall loss is plotted vs. the error in nozzle concentricity in the lower part of Figure 23. Here a linear correlation is seen, with a correlation coefficient of 0.94. The upper part of Figure 23 shows that the fine fraction is also linearly correlated with the error in nozzle concentricity. Although the wall losses are all less than 1%, the fine fraction ranges from about 3 to 18%. This variation could be eliminated by adherence to the specifications. The reason that the 3.0 μm data are sensitive to nozzle concentricity is probably because about 90% of the mass is in

TABLE 5. COARSE FRACTION, FINE FRACTION AND WALL LOSS OF DOP-URANINE PARTICLES IN DICHOTOMOUS SAMPLERS

Aerodynamic Dia., μm	Sampler	Serial No.	Coarse Fraction, %	Fine Fraction, %	Wall Loss, %	No. of Runs
2.0	Sierra	186	33.4 ± 3.1	65.3 ± 3.1	1.3 ± 0.1	3
	Sierra	151	33.5 ± 1.7	65.0 ± 1.8	1.5 ± 0.1	3
	Sierra	149	32.2 ± 2.5	66.8 ± 2.5	1.0 ± 0.2	3
	Ave.		33.0 ± 0.7	65.7 ± 1.0	1.3 ± 0.3	
	Beckman	038	31.7 ± 2.1	66.9 ± 2.1	1.4 ± 0.2	3
	Beckman	036	33.7 ± 3.1	64.8 ± 3.1	1.5 ± 0.2	3
	Ave.		32.7 ± 1.4	65.9 ± 1.5	1.5 ± 0.1	
	Average all Samplers		32.9 ± 0.9	65.8 ± 1.0	1.3 ± 0.2	
2.5	Sierra	186	54.2 ± 2.7	43.3 ± 2.4	2.6 ± 0.3	4
	Sierra	151	59.3 ± 3.0	38.7 ± 3.2	2.1 ± 0.2	3
	Sierra	149	58.0 ± 0.8	39.6 ± 1.2	2.3 ± 0.4	3
	Ave.		57.2 ± 2.7	40.5 ± 2.4	2.3 ± 0.3	
	Beckman	038	56.7 ± 4.4	41.0 ± 4.8	2.4 ± 1.0	4
	Beckman	036	60.8 ± 0.3	37.2 ± 0.7	2.0 ± 0.4	3
	Ave.		58.8 ± 2.9	39.1 ± 2.7	2.2 ± 0.3	
	Average all Samplers		57.8 ± 2.5	40.0 ± 2.3	2.3 ± 0.2	

TABLE 5 (continued)

TABLE 5 (continued)

Aerodynamic Dia., μm	Sampler	Serial No.	Coarse Fraction, %	Fine Fraction, %	Wall Loss, %	No. of Runs
3.0	Sierra	186	92.2 ± 2.5	7.3 ± 2.3	0.6 ± 0.1	2
	Sierra	151	81.8 ± 1.4	17.4 ± 1.5	0.9 ± 0.1	2
	Sierra	149	97.0 ± 1.3	2.7 ± 1.3	0.3 ± 0	2
	Ave.		90.3 ± 7.8	9.1 ± 7.5	0.6 ± 0.3	
	Beckman	038	86.3 ± 2.1	13.0 ± 2.0	0.8 ± 0.1	2
	Beckman	036	96.5 ± 2.0	3.3 ± 2.0	0.3 ± 0	2
	Ave.		91.4 ± 7.2	8.2 ± 6.9	0.6 ± 0.4	
	Average all Samplers		90.8 ± 6.6	8.7 ± 6.4	0.6 ± 0.3	
5.0	Sierra	186	99.7 ± 0.2	< 0.1	0.3 ± 0.1	2
	Sierra	151	99.7 ± 0.2	0.2 ± 0.2	0.2 ± 0.1	2
	Sierra	149	99.9 ± 0.1	< 0.1	0.1 ± 0.1	2
	Ave.		99.8 ± 0.1	0.1 ± 0.1	0.2 ± 0.1	
	Beckman	038	99.8 ± 0.1	< 0.1	0.1 ± 0.1	2
	Beckman	036	99.9 ± 0.1	< 0.1	0.1 ± 0.1	2
	Ave.		99.9 ± 0.1	< 0.1	0.1 ± 0.1	
	Average all Samplers		99.8 ± 0.1	< 0.1	0.2 ± 0.1	

TABLE 5 (continued)

TABLE 5 (continued)

Aerodynamic Dia., μm	Sampler	Serial No.	Coarse Fraction, %	Fine Fraction, %	Wall Loss, %	No. of Runs
10	Sierra	186	99.4 ± 0.1	0.1 ± 0.1	0.5 ± 0.1	3
	Sierra	151	99.6 ± 0.1	< 0.1	0.5 ± 0.1	3
	Sierra	149	99.6 ± 0	< 0.1	0.4 ± 0	3
	Ave.		99.5 ± 0.1	< 0.1	0.5 ± 0.1	
	Beckman	038	99.6 ± 0	< 0.1	0.4 ± 0.1	3
	Beckman	036	99.7 ± 0	< 0.1	0.3 ± 0.1	3
	Ave.		99.7 ± 0.1	< 0.1	0.4 ± 0.1	
	Average all Samplers		99.6 ± 0.1	< 0.1	0.4 ± 0.1	
15	Sierra	186	97.3 ± 0.6	< 0.1	2.7 ± 0.6	3
	Sierra	151	93.9 ± 0.9	0.1 ± 0.1	6.1 ± 1.0	3
	Sierra	149	97.1 ± 0.4	< 0.1	2.9 ± 0.5	3
	Ave.		96.0 ± 1.9	< 0.1	3.9 ± 1.9	
	Beckman	038	96.8 ± 1.0	0.1 ± 0.1	3.2 ± 1.0	3
	Beckman	036	95.9 ± 1.6	< 0.1	4.1 ± 1.4	3
	Ave.		96.4 ± 0.6	0.1 ± 0.1	3.7 ± 0.6	
	Average all Samplers		96.2 ± 1.4	< 0.1	3.8 ± 1.4	

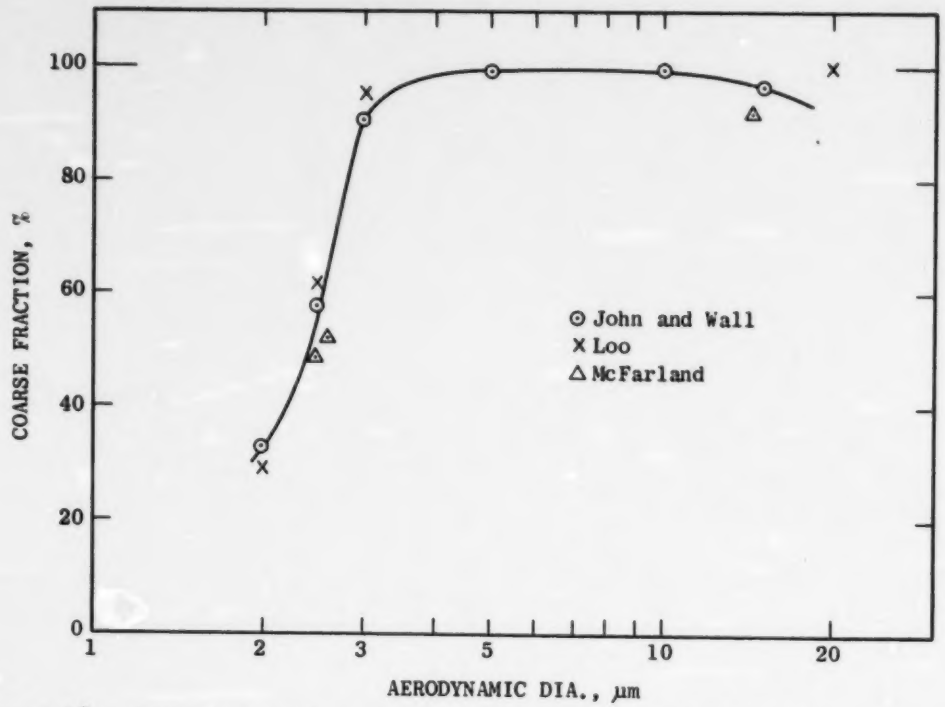

Figure 18. Coarse fraction vs. particle size for the dichotomous sampler. John and Wall data are average for 3 Sierra and 2 Beckman samplers using DOP-uranine; Loo data are average for 10 Beckman samplers and DOP-uranine; McFarland data are average of 10 Beckman samplers and oleic acid-uranine.

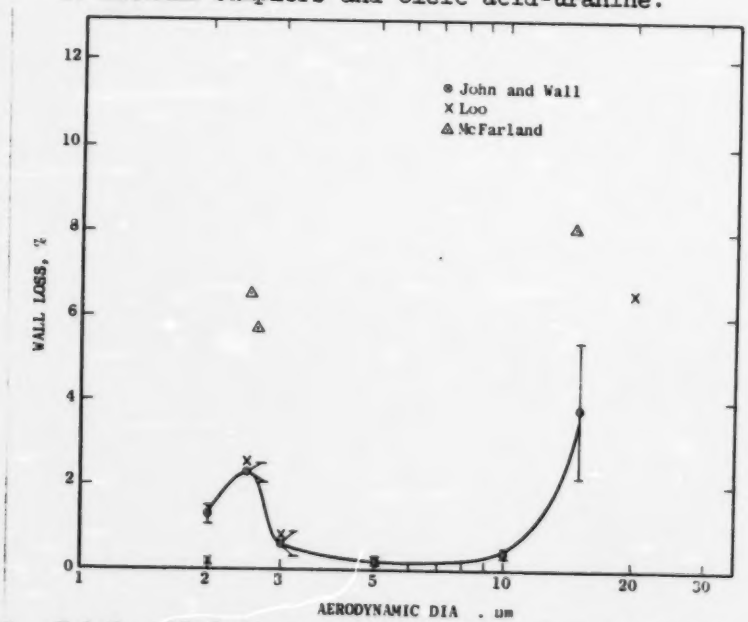

Figure 19. Total wall loss vs. particle size for the dichotomous sampler. See legend under Figure 18 for data identification.

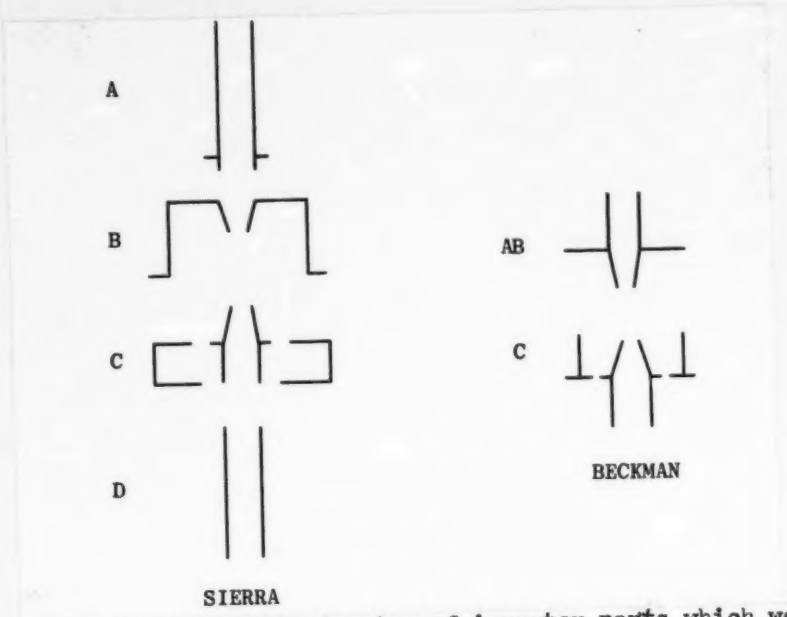

Figure 20. Schematic drawing of impactor parts which were washed separately to recover wall losses.

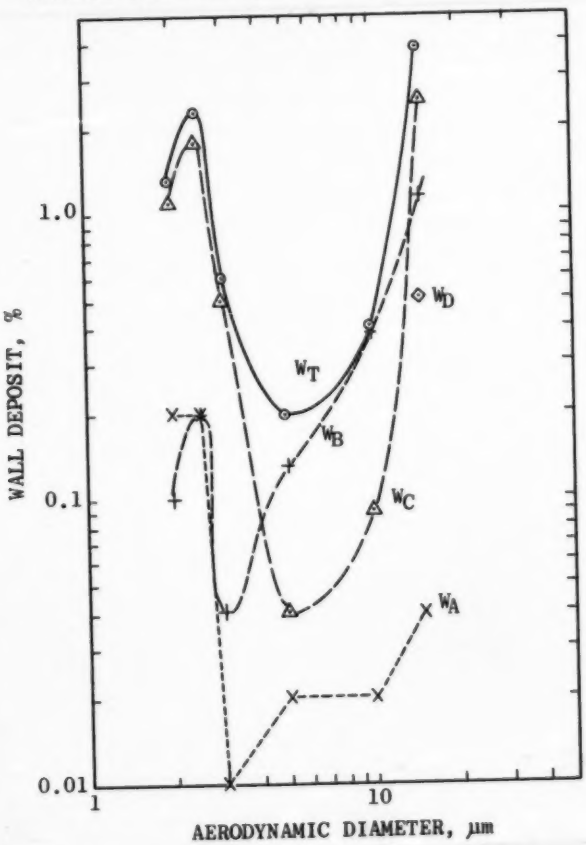

Figure 21. Wall losses measured for individual parts of the dichotomous sampler, labelled as in Figure 20. W_T = Total wall loss ($W_A + W_B + W_C + W_D$).

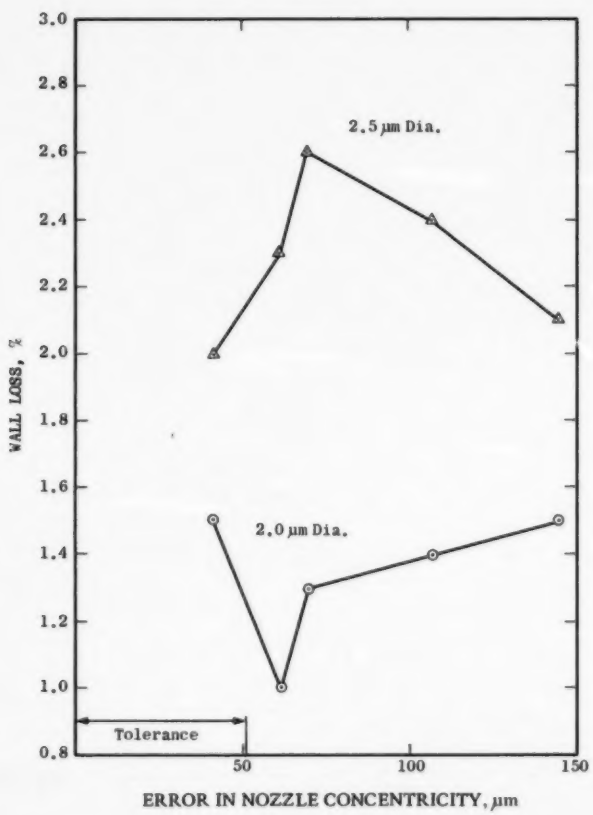

Figure 22. Total wall loss vs. error in concentricity for 2.0 and 2.5 µm dia. DOP-uranine particles.

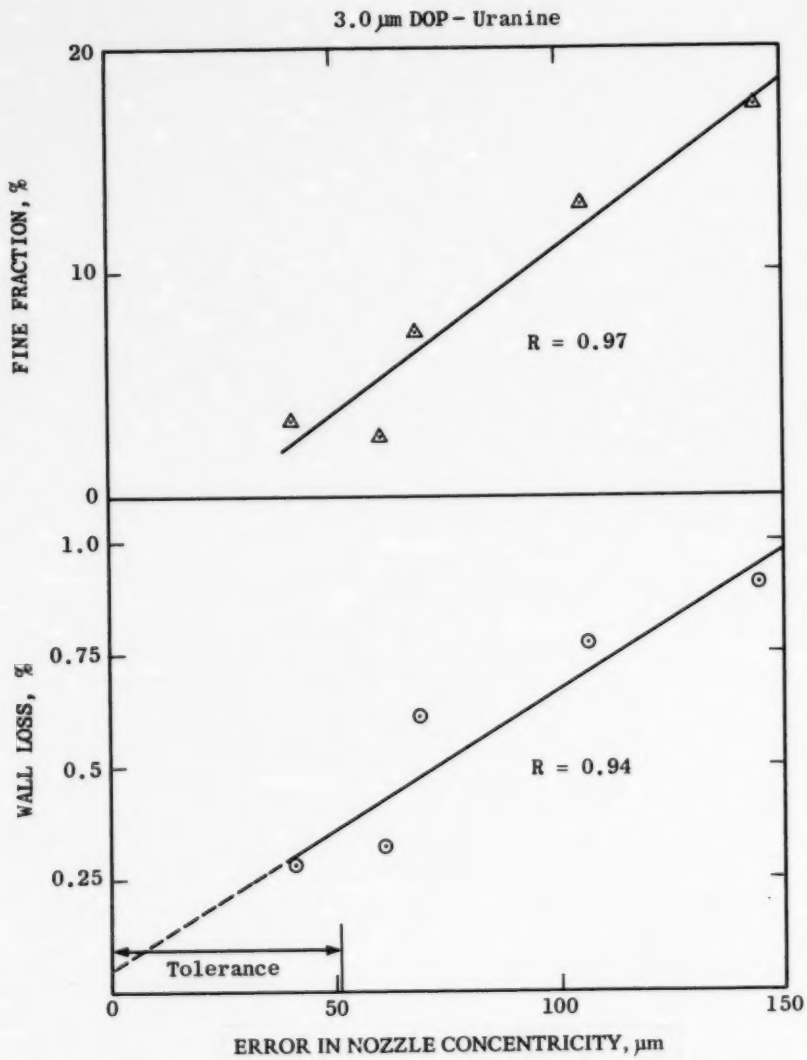

Figure 23. Upper half: fine fraction vs. error in nozzle concentricity. Lower half: wall loss vs. nozzle eccentricity. Both were measured with 3.0 μm particles. Regression lines and correlation coefficients are shown.

the coarse fraction at this particle size. To reach the collection nozzle, the particles must cross almost all of the streamlines. A small error in nozzle alignment will allow particles to escape to the fine fraction.

In Figure 24, the wall loss is plotted vs. the fine fraction for particle diameters of 2.0, 2.5 and 3.0 μm. For 2.5 μm and 3.0 μm particles, the wall losses increase with fine fraction as expected, since a larger fine fraction means that more particles will pass near the lip of the collection nozzle. At 2.0 μm there is a weak negative correlation since 2.0 μm particles are below rather than above the 50% cutpoint.

To investigate the possibility that the wall loss depends on the mass loading, measurements were made with up to nearly 3 mg of 2.5 μm particles. Both oleic acid and DOP particles were used to detect any possible difference resulting from the fact that uranine dye is soluble in oleic acid but not in DOP. From Figure 25 it can be seen that the wall loss is insensitive to mass loading, the data showing a very slight decrease with loading. Also, the oleic acid and DOP results are identical within the error.

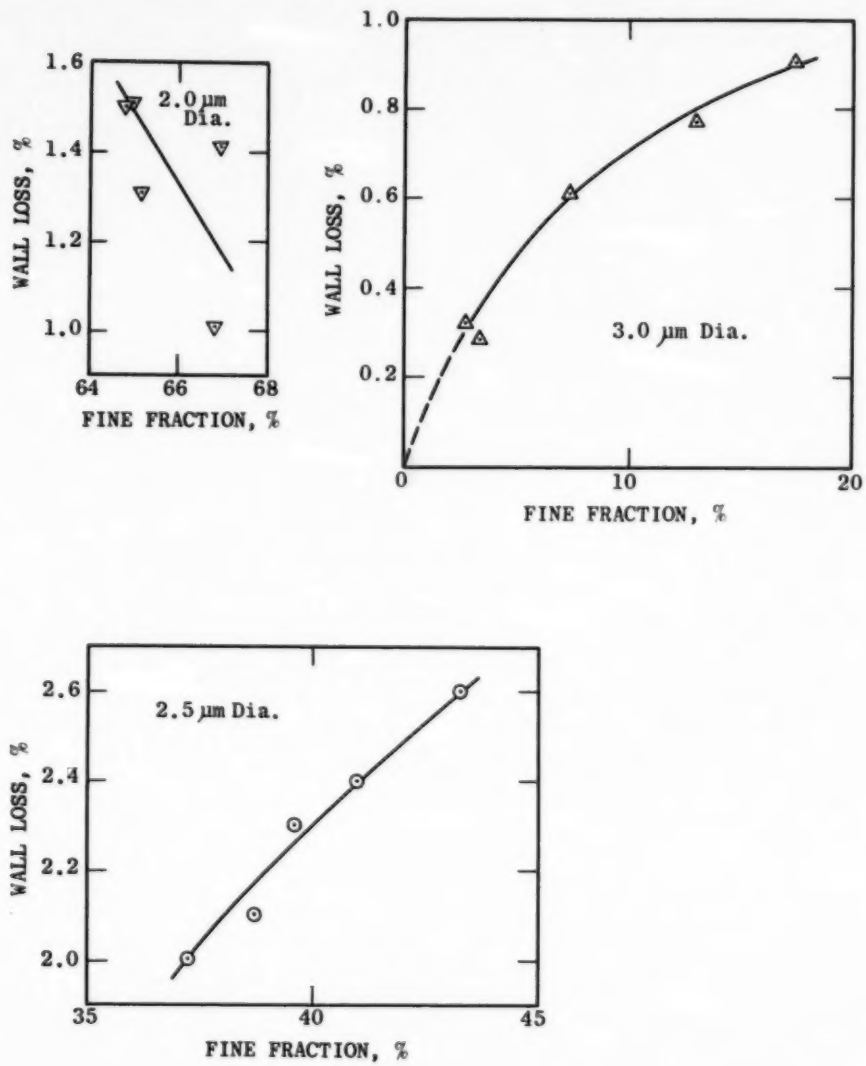

Figure 24. Wall loss vs. fine fraction for 2.0, 2.5 and 3.0 μm dia. DOP-uranine particles.

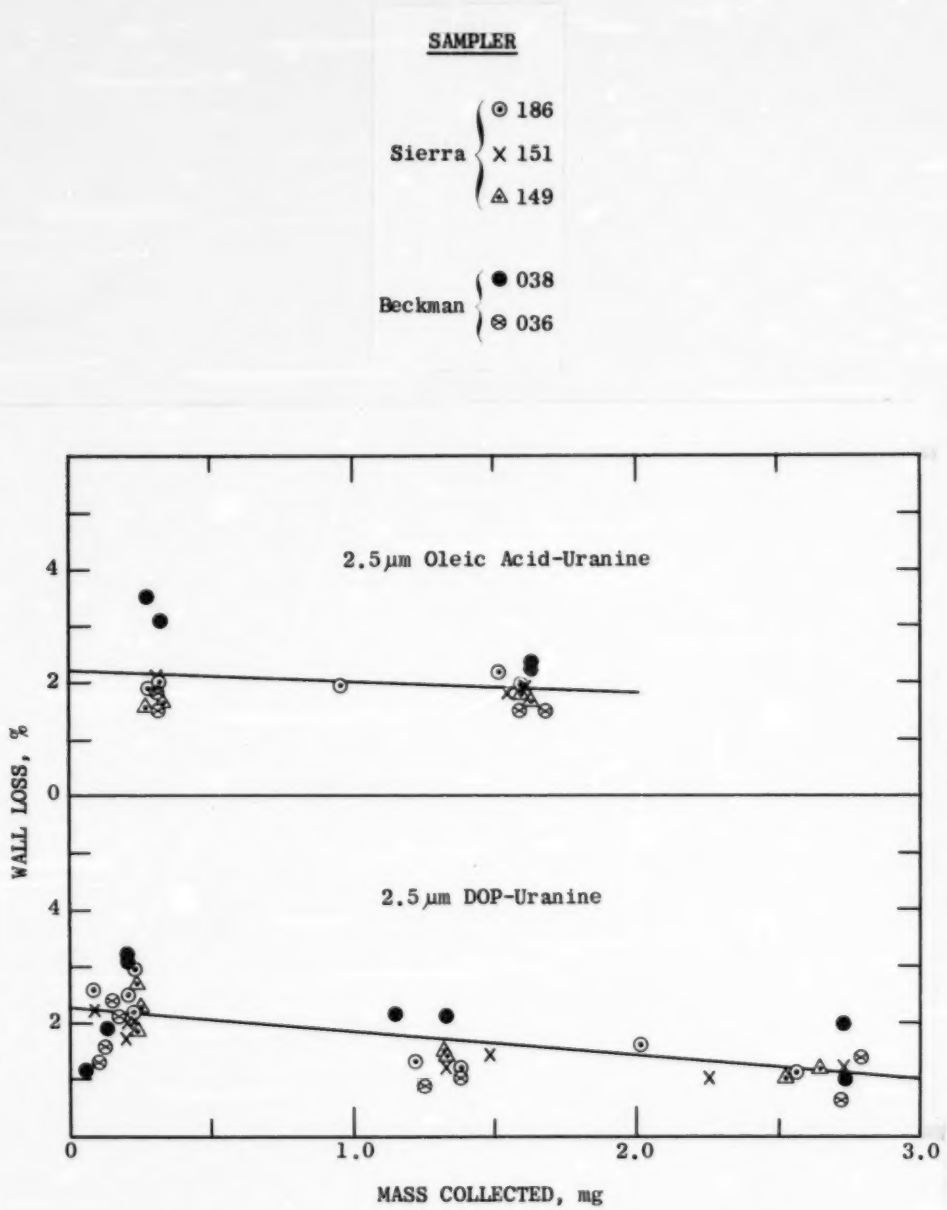

Figure 25. Wall loss vs. mass loading with oleic acid particles (top) or DOP particles (bottom).

SECTION 6

TESTING OF THE SIZE-SELECTIVE HI-VOL

The size-selective hi-vol employs a new type of inlet to convert a standard hi-vol to an inhalable particle sampler. Because the high flow rate affords a large sample for chemical analysis, this sampler is being tested in the EPA Inhalable Particle Network. The present work investigated the sampling characteristics for solid particles, including penetration to the filter because of bounce and reentrainment.

The sampler consists of a size-selective inlet (SSI) (14) which replaces the roof of a conventional hi-vol (Figure 26). A set of nine acceleration nozzles facing an aluminum plate constitutes an inertial impactor which, combined with the effects of the 16 collection tubes, results in a 50% cutpoint at 15 μm. The collection tube geometry is intended to prevent reentrainment of particle deposits. Results of wind tunnel tests on the size-selective hi-vol indicate that variation of sampling efficiency with particle size and wind speed is acceptable, according to EPA criteria (14,15). Additional data on the performance are sparse.

Since the sampler employs a smooth aluminum impaction plate, the possibility of particle bounce and reentrainment is of concern. The present testing used solid, spray-dried particles to measure excess particle penetration in the vicinity of the cutoff and glass beads to measure penetration well beyond the cutoff. Arizona road dust was also used for tests. Ambient clay dust was sampled and large particle penetration studied by microscopy. A summary of other important characteristics of the size-selective hi-vol, measured by the authors (16) under the sponsorship of the California Air Resources Board, is included for completeness.

DIMENSIONS

Measurements were made on the key dimensions (Figure 27) of the sampler which was tested. These are summarized in Table 6. Most of the dimensions agree well with the EPA specifications with the exceptions of dimensions E and H. However, these errors were judged not to affect performance. The sampler was considered representative for testing purposes.

SOLID PARTICLE PENETRATION NEAR THE CUTOFF

This test is basically a comparison between the sampling effectiveness for liquid particles and solid particles of the same aerodynamic diameter, in

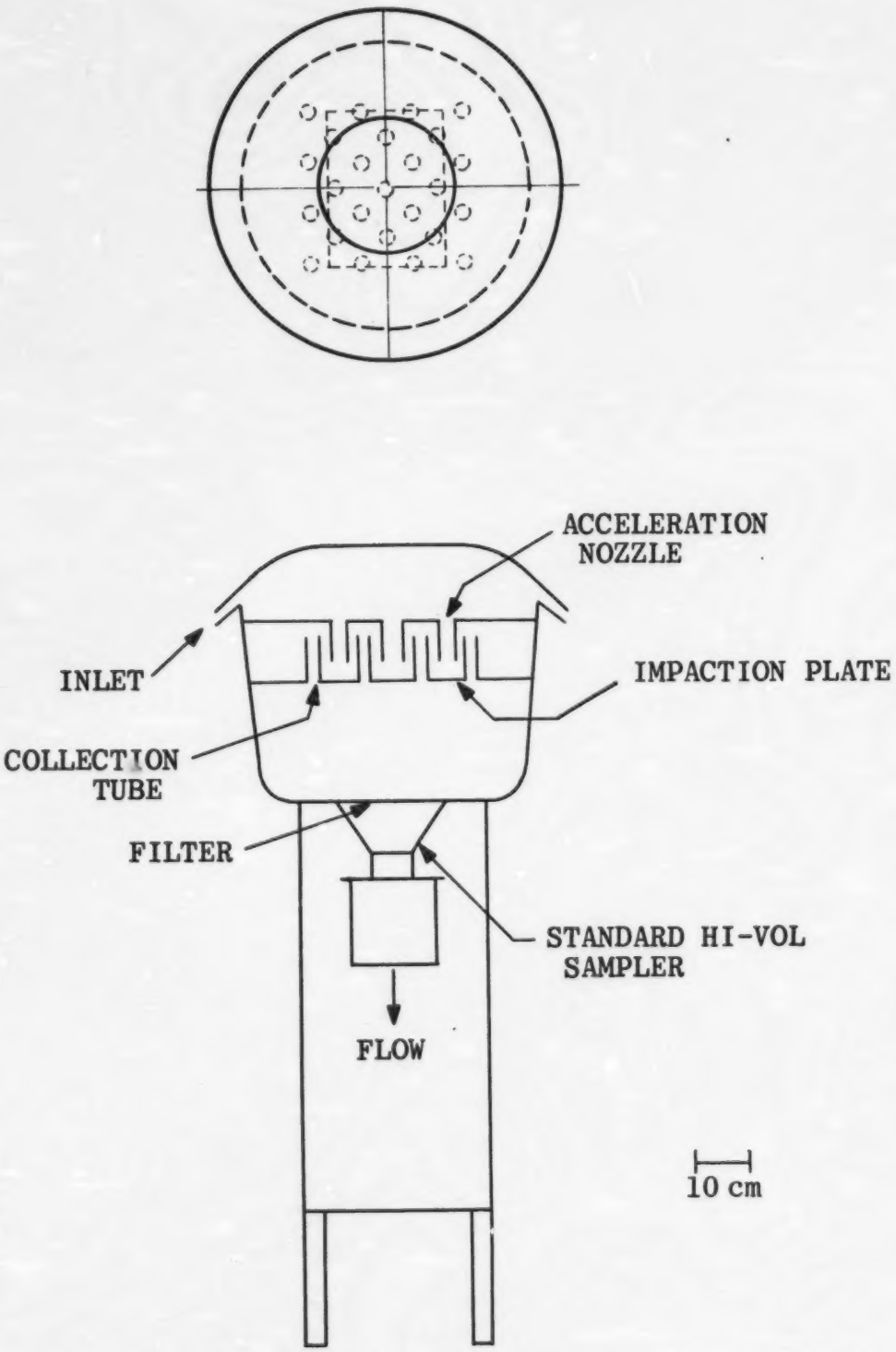

Figure 26. Size-selective hi-vol sampler.

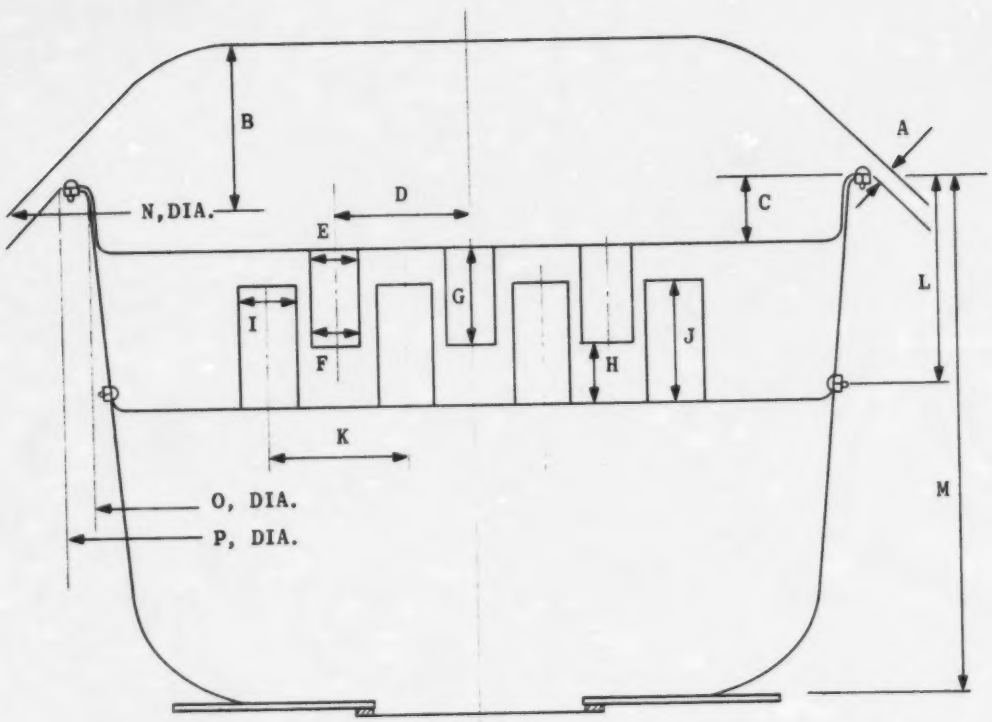

Figure 27. Key for dimensional measurements of the size-selective hi-vol listed in Table 6.

TABLE 6. DIMENSIONS (IN INCHES) OF THE SSI TESTED IN THE PRESENT WORK[a]
See Figure 27 for Location Key

Location	Specification[b]	Ave. measured dimension ± std. dev.	Precision[c]
A Inlet gap spacer (4)	0.75	0.750 ± 0.001	0.001
B Inlet dome height	4.8	4.820 ± 0.001	0.001
C Acceleration nozzle plate detent	1.80	1.899 ± 0.007	0.001
D Acceleration nozzle spacing (9 nozzles)	4.0	3.98 ± 0.03	0.001
E Acceleration nozzle inlet I.D.	1.444	1.421 ± 0.002	0.002
F Acceleration nozzle exit I.D	1.444	1.426 ± 0.004	0.002
out of round[d]	--	0.003 ± 0.003	0.002
G Acceleration nozzle length	2.83	2.825 ± 0.004	0.003
H Acceleration nozzle to impaction plate spacing	--	1.439 ± 0.019	0.002
I Collection tube I.D. (16 tubes)	1.380	1.381 ± 0.003	0.002
J Collection tube length	3.48	3.465 ± 0.005	0.001
K Collection nozzle spacing	4.0	4.00 ± 0.01	0.001

TABLE 6 (continued)

TABLE 6 (continued)

	Location	Specification[b]	Ave. measured dimension std. dev.	Precision[c]
L	Impaction plate bolt hole height	5.685	5.686 ± 0.002	0.002
M	Chamber height	14.6	14.6 ± 0.1	0.06
N	Inlet dome dia.	27.6	27.63 ± 0.03	0.03
O	Chamber dia.	22.00	22.0 ± 0.10	0.06
P	Chamber and flange dia.	24.0	24.0 ± 0.1	0.06

Notes: [a]Sierra Instruments Model UV-5H.

[b]EPA specifications based on drawings from Texas A & M University.

[c]The precision applies to measurement of a single part or at one location.

[d]Difference of measurements at 90° to each other.

order to detect any excess penetration by solid particles. Since the effectiveness falls off steeply in the vicinity of the cutpoint, the particles must be highly monodisperse and accurately sized. These requirements were met by spray-drying potassium biphthalate (KHP) solution from a Berglund-Liu aerosol generator. Because the KHP particles do not dry to bulk density, it was necessary to measure their aerodynamic diameter, which was done with a Laser Sedimentation Velocimeter.

The size-selective hi-vol (SSI) sampled aerosol from an enclosure as shown in Figure 28. The incoming aerosol was sampled isokinetically just inside the inlet of the SSI onto 25 mm Teflon membrane filters as shown in Figure 29. The KHP particles contained 1% uranine dye tracer. Recovery from the 8" x 10" glass fiber filter was accomplished by separating the fibers in water with a blender and vacuum filtering the slurry. An Aminco fluorometer was used to quantitate the uranine content. Sampling effectiveness was computed from the measured filter deposits with appropriate correction for flow rates.

Results for the solid KHP particles are plotted in Figure 30. These are to be compared to the results for liquid DOP particles taken under similar conditions. A small excess penetration by the solid particles is observed, amounting to 25% at the cutpoint. This is not deemed to be serious for two reasons. First, the 50% cutpoint for KHP particles is 17 µm, compared to 15 µm for liquid particles. This would result in a relatively small error in sampled mass, ordinarily. Secondly, KHP particles are bouncier than most particles expected in ambient air. Figure 30 also includes data from wind tunnel measurements with liquid particles at low wind speed (2 km/hr). The present zero wind speed data are in reasonably good agreement.

PENETRATION BY LARGE PARTICLES

Excess penetration by large, bouncy particles is of concern due to their large contribution to mass (e.g. a 60 µm diameter particle has the mass of 64 15 µm diameter particles). Sampling effectiveness measurements in the range 30-70 µm aerodynamic diameter were made using glass beads* and A/C test dust**. These materials were chosen to model large wind-blown soil particles. Solid glass spheres have a density and elemental composition similar to common soil minerals, but have a higher potential for bounce and reentrainment due to their high elasticity. A/C test dust consists of sized soil aggregates which have a potential for breakup and reentrainment. Test aerosols of these materials allow a worst case evaluation of sampler performance.

*Uniform Glass Microspheres obtained from the Duke Scientific Corp., Palo Alto, CA.

**A/C Fine Test Dust obtained from the Duke Scientific Corporation.

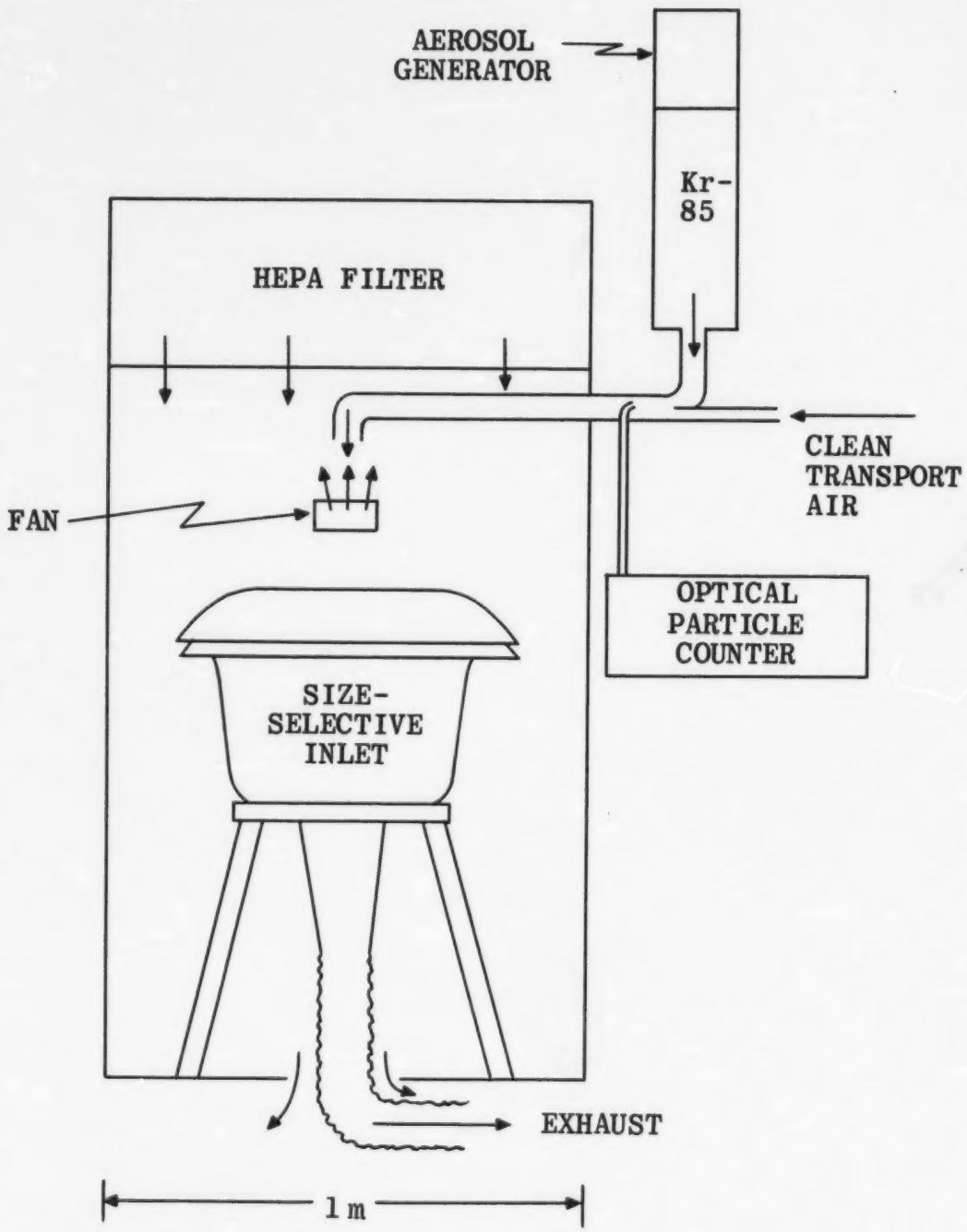

Figure 28. Experimental arrangement for measurement of penetration of the SSI by spray-dried solid particles.

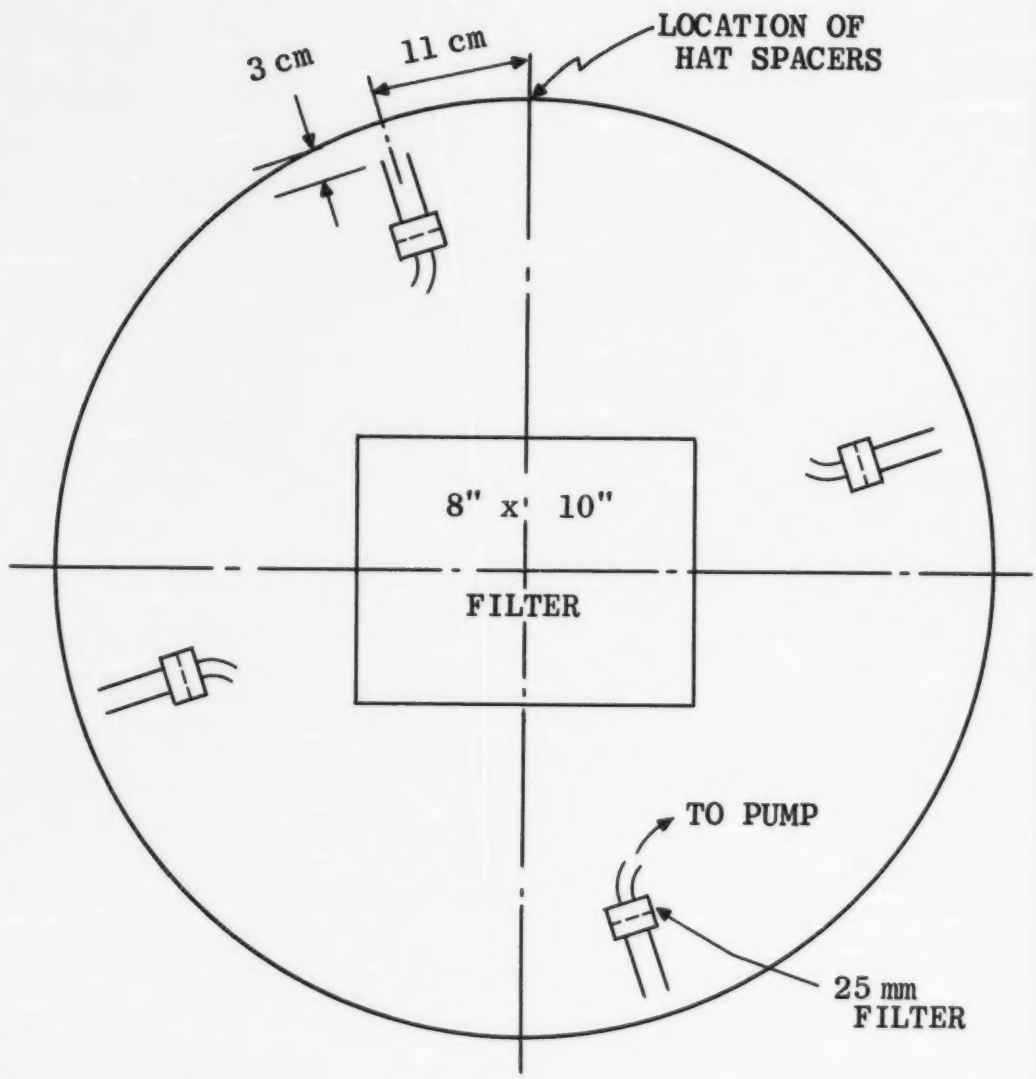

Figure 29. Location of 25mm prefilter samplers inside the size-selective hi-vol.

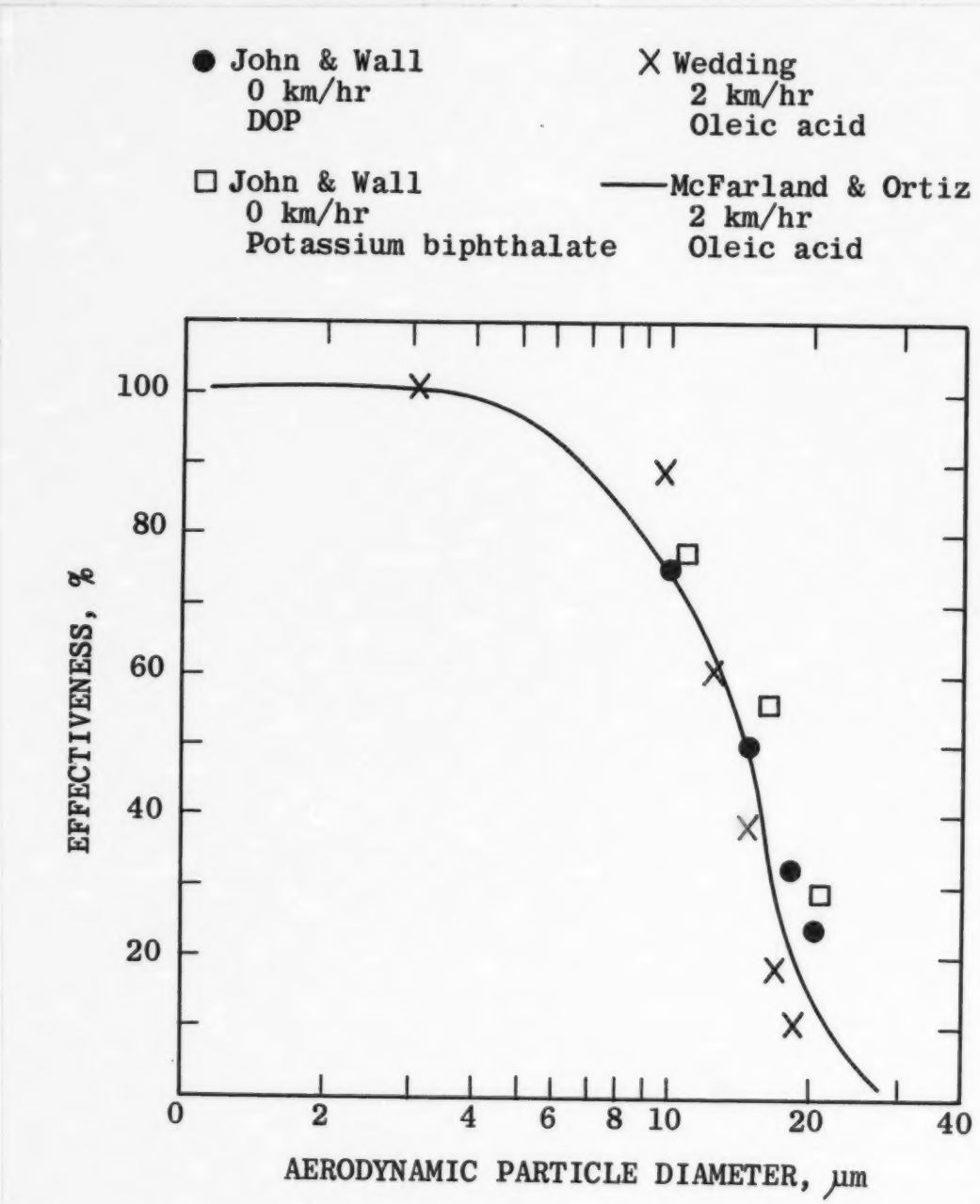

Figure 30. Sampling effectiveness of the size-selective hi-vol measured in the present work at zero wind speed for liquid (DOP) and solid (potassium biphthalate) particles. Data from wind tunnel tests at 2 km/hr wind speed are shown for comparison.

Sonic Fluidized Microbed Generator

Aerosol generation from these dry bulk materials required a system for deagglomeration and dispersal of individual particles as well as neutralization of their electrical charge. A novel Sonic Fluidized Microbed generator (SFM) was developed for this application (Figure 31). The particles to be aerosolized are placed in a bed of 177-212 μm glass beads at the base of a thin Mylar cone. The bed is supported on a 25 mm dia., 0.8 μm pore size Nuclepore filter through which the fluidizing air is passed. A piezoelectric crystal suspended from the Nuclepore filter is used to vibrate the bed particles (See Fig. 32). This eliminates the common problem of channeling of air through small regions of the bed. The diverging sides of the funnel create an upward air velocity gradient which stratifies particles based on their settling velocity enabling finer control of the elutriation of particles from the generator. Piezoelectric crystals vibrate the Mylar bed walls at 9 Khz to prevent particle adhesion. Po-210 strips are used to ionize the incoming dilution air in order to reduce the charge on the aerosol.

An outstanding feature of the SFM is the small quantity of material required for operation. Typically 1g of bed beads and < 0.5 g of test particles are utilized which makes it feasible to use small amounts of expensive pre-sized test particles. Bed beads may also be discarded after each run to avoid cross contamination with the next particle charge.

The SFM flow rate required to generate aerosols from pre-sized solid glass micro beads is shown in Figure 33. The error bars reflect the spread in the diameter of the pre-sized particles, rather than the reproducibility of the generated aerosol size. The SFM obeys vertical elutriator theory (solid line) when the bed particles are omitted. The use of glass bed beads allowed larger diameter aerosols to be produced at lower flow rates. Bed beads 177-212 μm proved to be optimum for these studies. For this size bed particles, the SFM operating conditions can be estimated from $D_{Aero} = 5.7\ Q + 10.4$, where D_{Aero} is the mean aerodynamic particle diameter in μm and the flow rate Q is in L/min. Measurements were made to compare the size distributions of the test aerosol and the bulk glass beads from which they were generated (Table 7). Particles were sized by light microscopy using a traveling hair line eyepiece. The results indicate little change in the mean diameter but there is some evidence that the SFM narrows the size distribution.

Large Particle Penetration Measurements

The experimental configuration used to investigate the importance of large particle penetration in the size-selective hi-vol is shown in Figure 34. The sampler was mounted in a test chamber with a vertical flow of clean air from a HEPA filter with the excess flow vented through the bottom of the chamber rear wall. The top cover of the sampler inlet was removed and the SFM generator placed directly over the inlets of two acceleration nozzles (Figures 35,36). The generator enclosure was open at the top to eliminate restrictions to the sampler air flow. The aerosol concentration entering the inlet was monitored with a 47 mm prefilter sampler attached to the outlet of the first acceleration nozzle, and operated at the normal nozzle flow rate. Aerosol which entered the second acceleration nozzle and penetrated the inlet was monitored

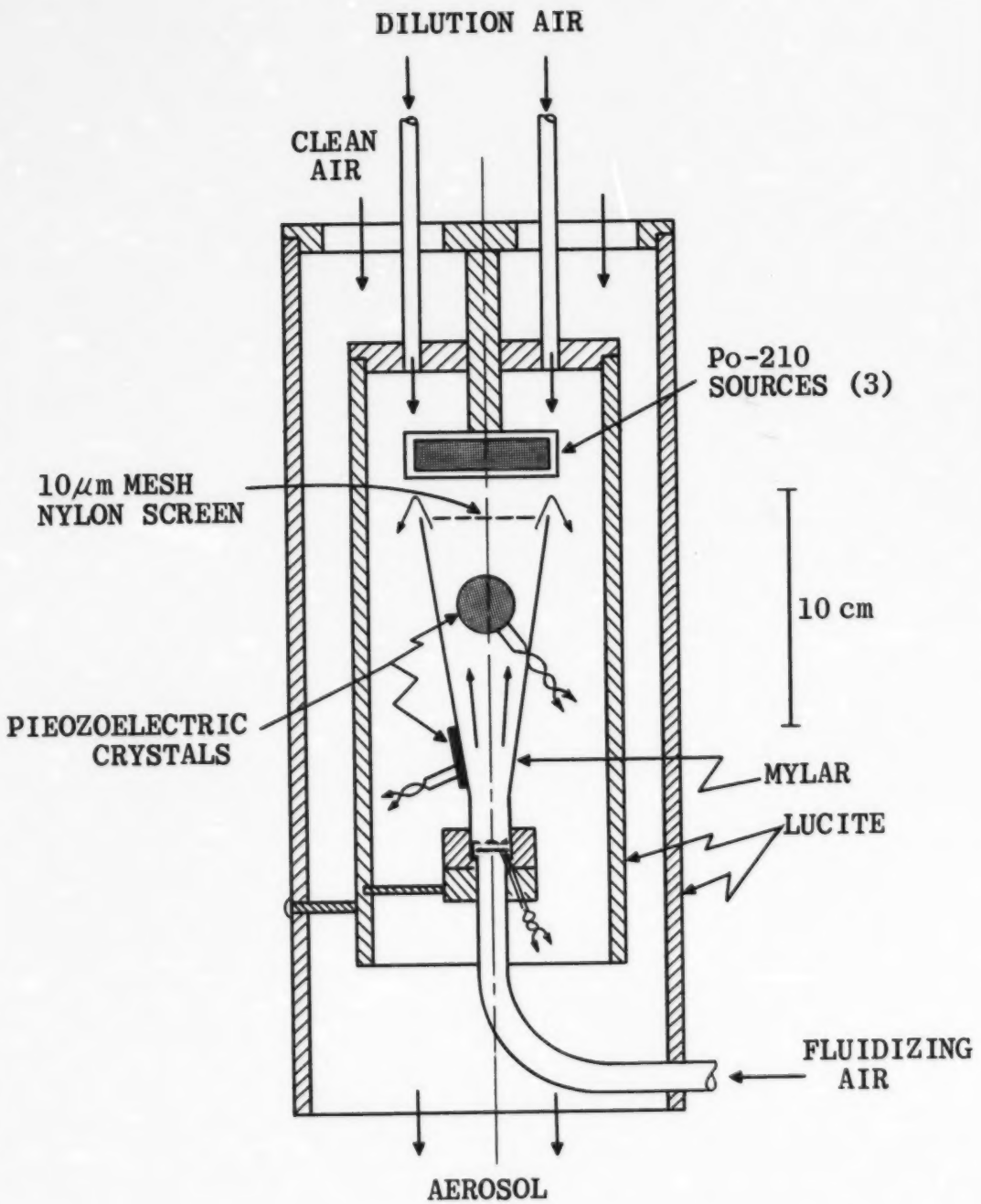

Figure 31. Schematic drawing of the sonic fluidized microbed generator.

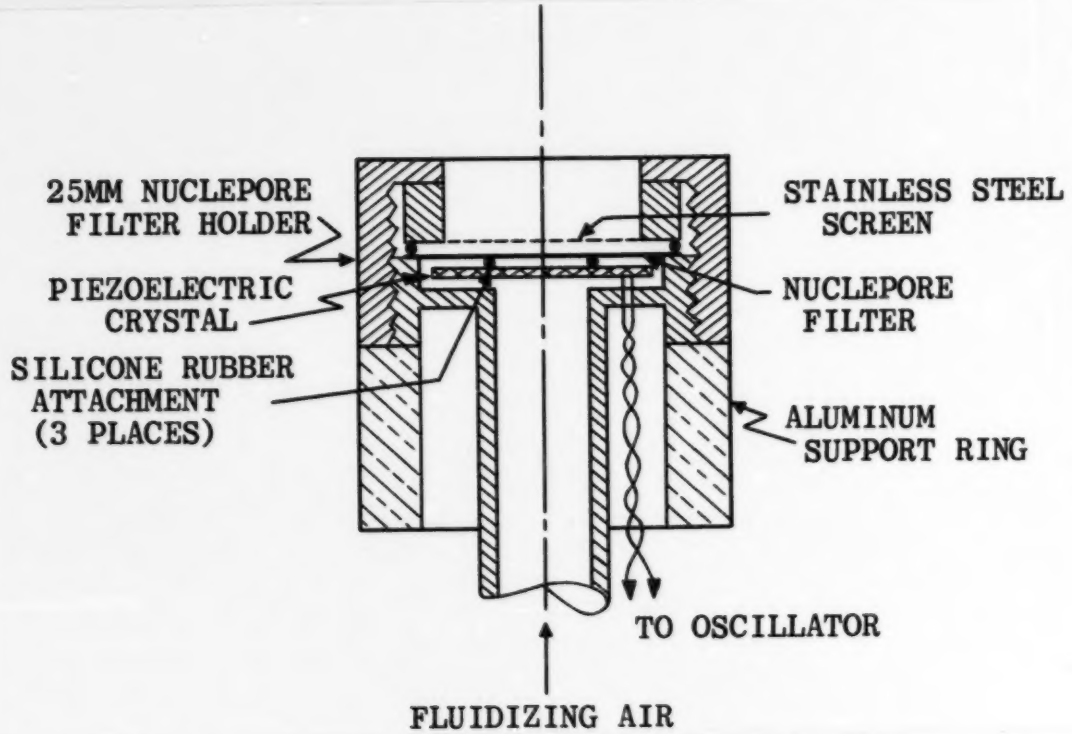

Figure 32. Detail of the base of the sonic fluidized microbed generator.

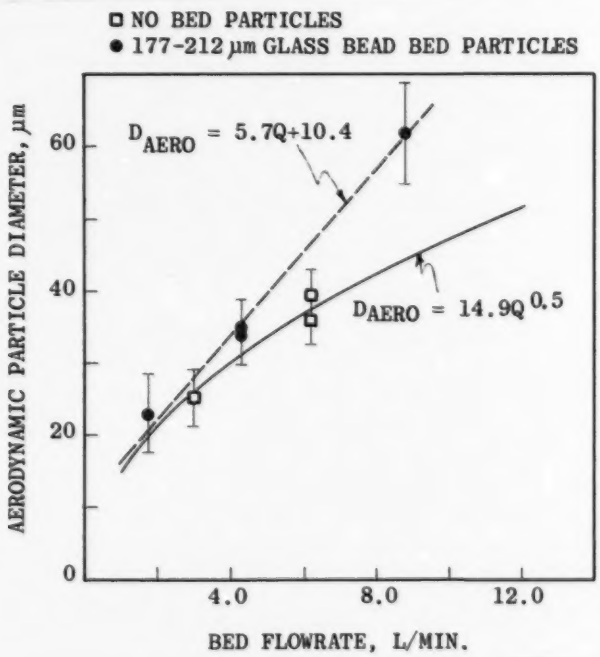

Figure 33. Mean aerodynamic diameter of the particles from the sonic fluidized microbed generator vs. the bed flowrate.

TABLE 7. SIZES OF GLASS BEADS AND AEROSOL GENERATED

Diameter Specified µm[b]	Treatment	Geometric Diameter, µm[a] Beads	Aerosol
10-20	Sieved[c]	15.7 ± 2.6	14.6 ± 3.5
20	Presized	20.0 ± 1.8[b]	22.0 ± 2.0
15-25	Presized	19.5 ± 5.0	22.1 ± 3.6
20-30	Sieved[c]	22.4 ± 4.1	21.5 ± 2.8
37-44	Presized	38.4 ± 7.0	39.8 ± 6.3

[a]Measured by optical microscopy

[b]Manufacturers specification

[c]Sieved from 1-37 µm diameter beads with sonic sifter

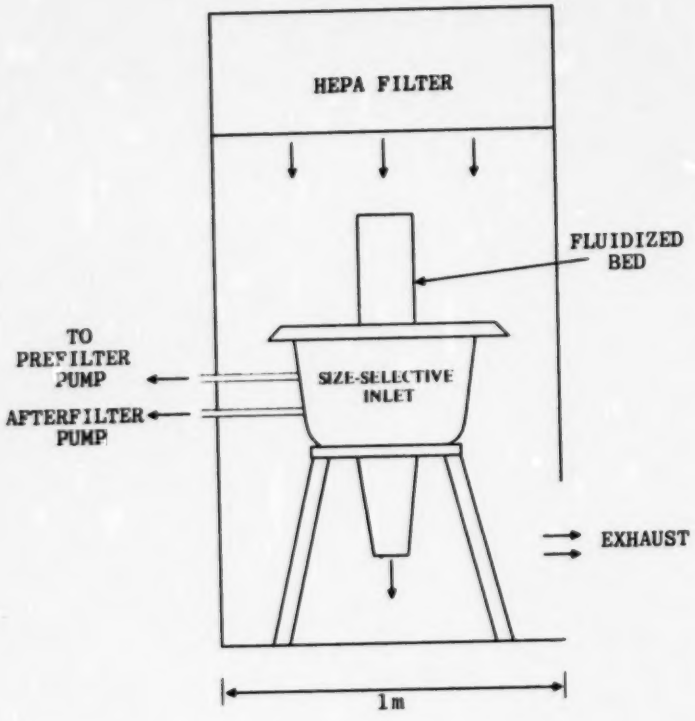

Figure 34. Experimental arrangement for testing the SSI with aerosol from the sonic fluidized microbed generator.

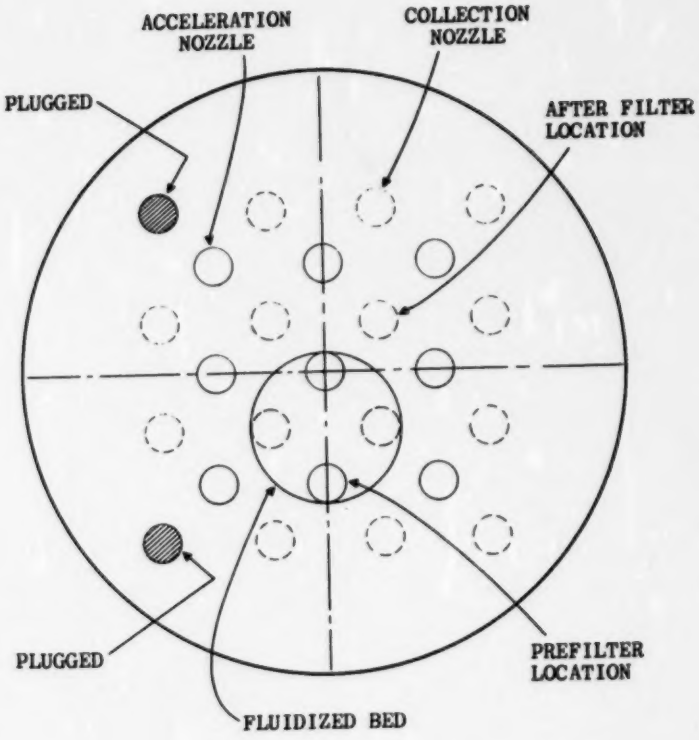

Figure 35. Location of the fluidized bed, prefilter and after filter in the SSI.

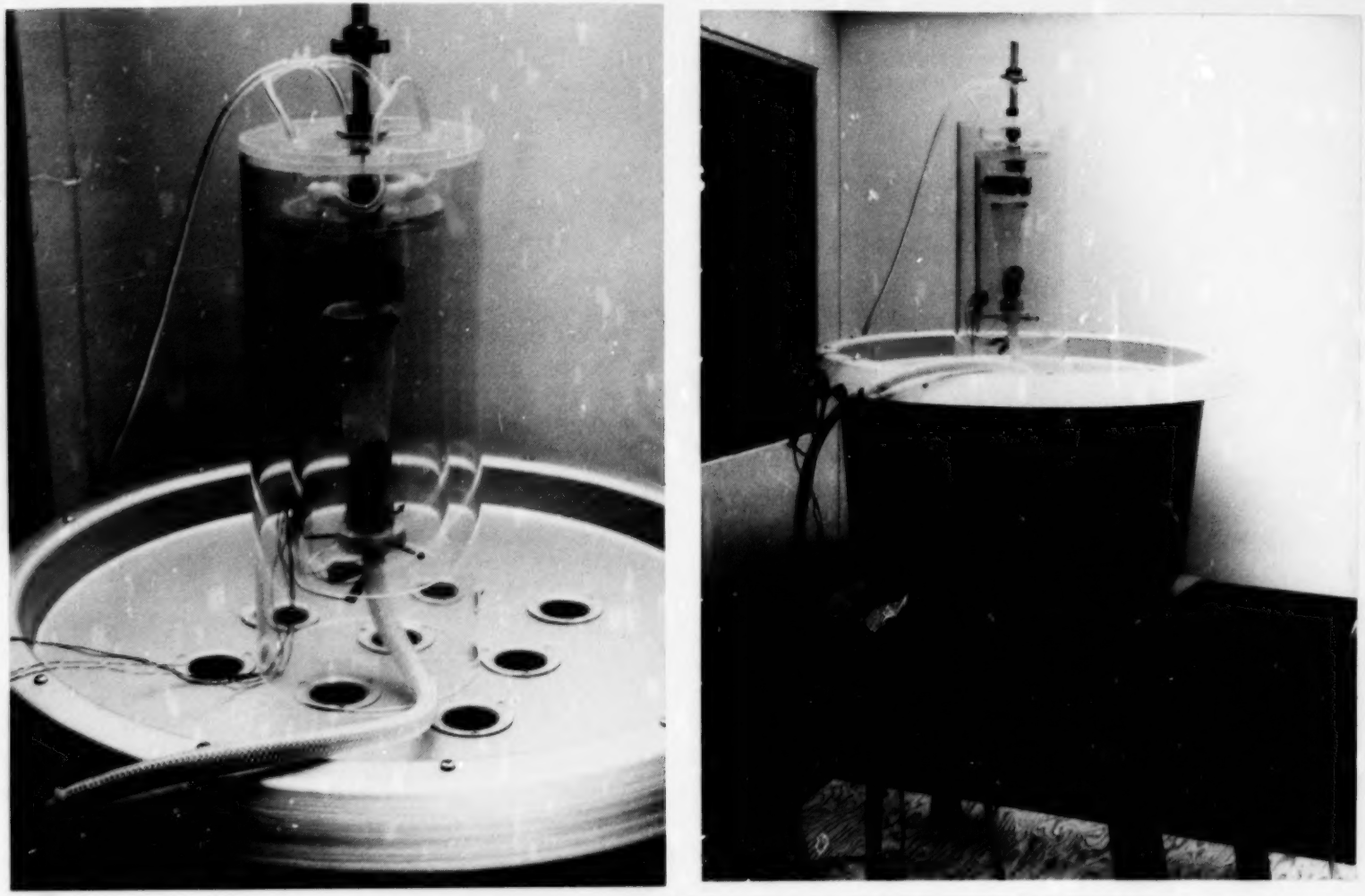

Figure 36. Photographs of the sonic fluidized microbed generator on the SSI for testing with glass beads and A/C test (Arizona road) dust.

by a 47 mm isokinetic after filter sampler. The after filter sampler was attached to the outlet of one of the four collection tubes associated with the second acceleration nozzle. To correct for changes in flow velocities within the inlet created by the introduction of the filter samplers, the inlet was operated at reduced flow rate (33 CFM) and two collection tubes were plugged.

The two acceleration nozzles sampled an equal mass of test aerosol within 11% as established with parallel prefilter sampling. Penetration efficiency was calculated by dividing four times the after filter loading by the prefilter loading. For these 47 mm filter samplers, 1 µm pore size Teflon membrane (Fluoropore) were used and filter loadings were determined gravimetrically with a microbalance (Cahn Model 26). Typically 30 mg (range 14-230 mg) of test particles were collected on the prefilter with 0.2 mg on the after filter.

Glass bead test particles collected on the 47 mm filter samplers were sized with an optical microscope equipped with a traveling hair line eye piece. Size frequency distributions obtained from the prefilter and after filter are shown in Figures 37 and 38 for two different diameter glass test particles. One hundred particles were counted for each distribution so peak heights are unrelated to penetration efficiency. The large particle peak in the after filter distribution represents particles which have penetrated the sampler by bounce and reentrainment. The small particle peak observed for both after filter samples is probably the result of the overlap of the tail of the glass bead size distribution with the inlet cut off curve. This small particle mode accounted for less than 3% of the after filter mass loading.

The highly agglomerated structure of the A/C test dust prevented accurate sizing. For bounce testing, this material was size classified by screening in a sonic sifter. The measured penetration efficiencies for particles above the SSI cutpoint are shown in Figure 40. As the SSI was operated without the top cover, these values should be considered upper limits of the particle penetration. Penetration of 3 to 4% by mass was observed for both glass beads and A/C test dust, which is acceptable for practical purposes. The A/C test dust point for 62 µm particles may be high due to particle break up on impaction surfaces within the inlet. (Such breakup may also occur with ambient particles.)

The small penetration of large solid particles does not imply that particle bounce is absent in the SSI. Visual examination indicated that few of the A/C test dust particles or glass beads were deposited on the impaction surface directly below the acceleration nozzle. Instead, the deposits were closer to the bases of the collection tubes as shown in the photographs of Figure 39. Apparently, particles which impacted below the jets bounced but were subsequently trapped in eddies near the bases of the collection tubes. This indicates that the SSI is not a conventional impactor but operates by a combination of mechanisms including impaction, turbulent deposition and gravitational settling.

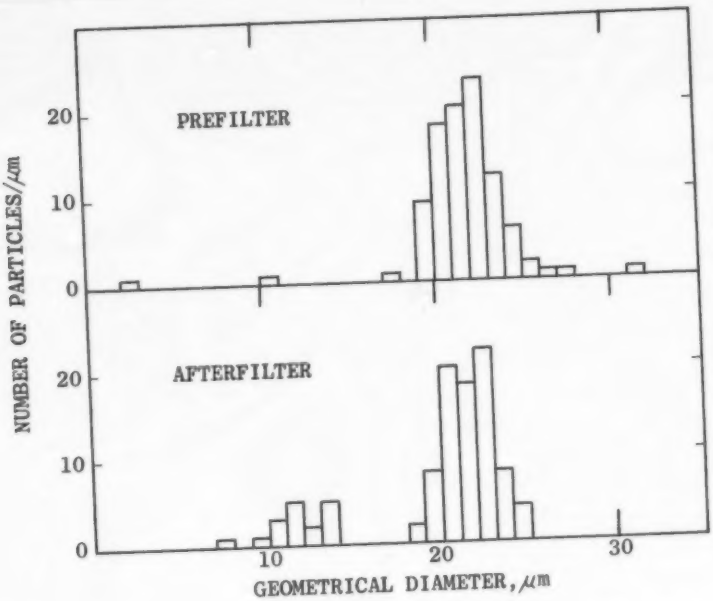

Figure 37. Size distributions of glass beads on the prefilter and after filter inside the SSI.

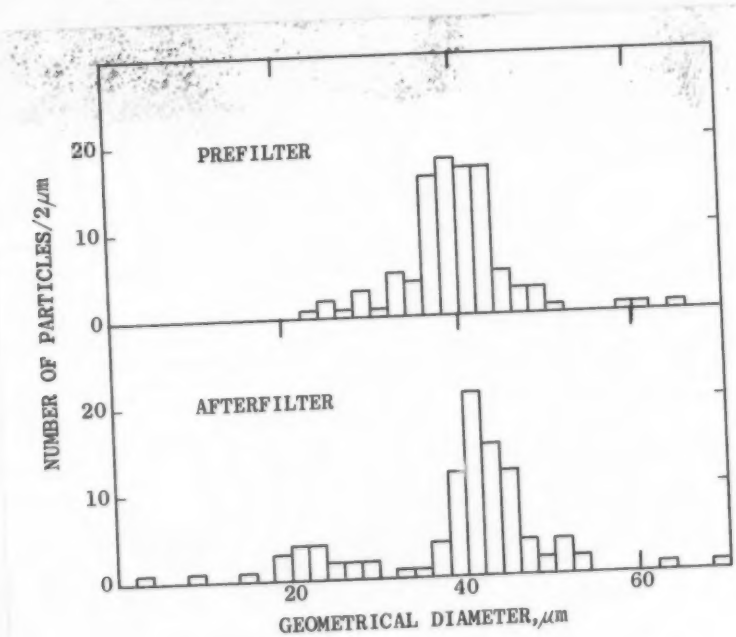

Figure 38. Same as Fig. 37 but with larger glass beads.

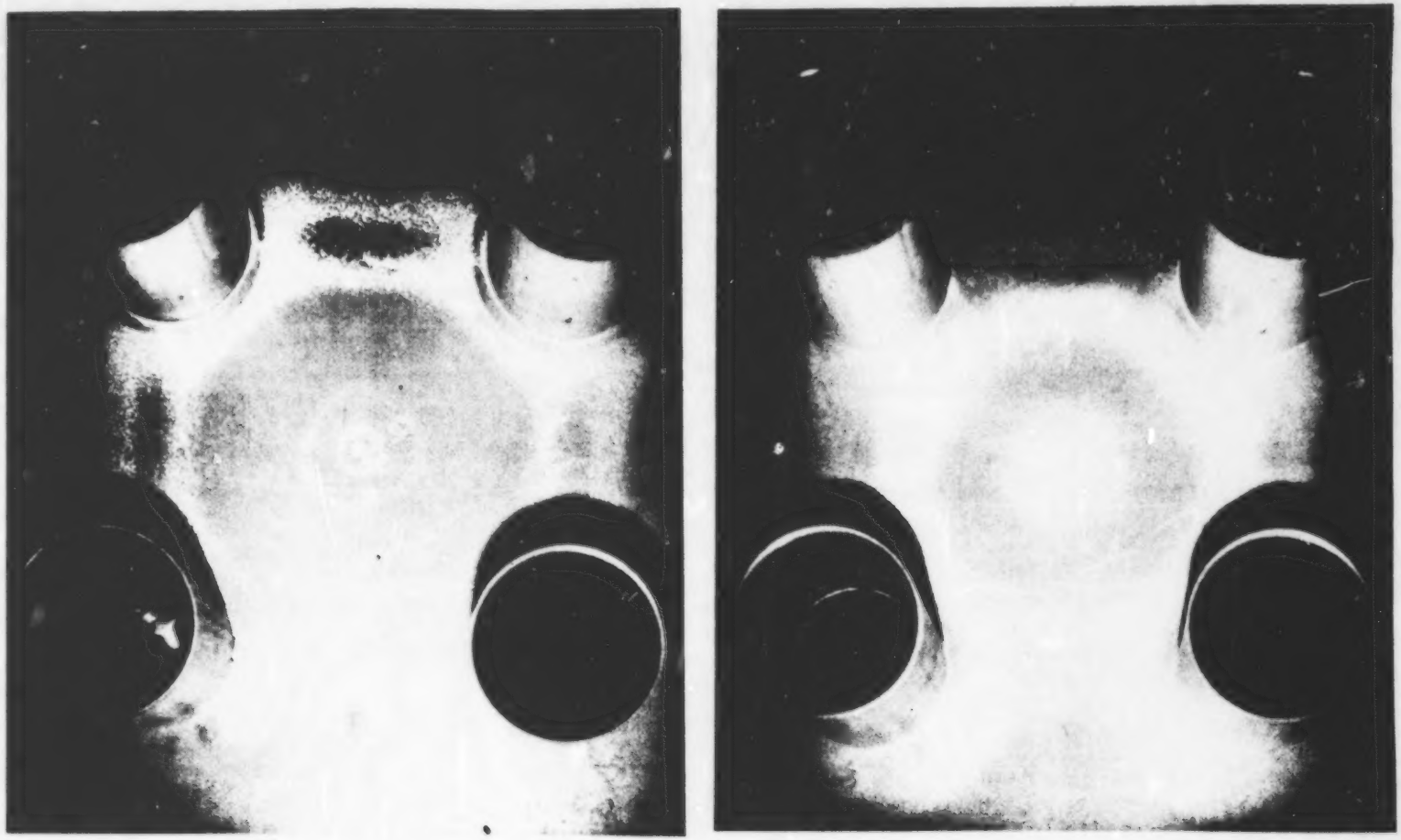

Reproduced from best available copy.

Figure 39. Photographs of glass bead deposits on the impaction plate of the SSI, with 40 μm beads (left) and 22 μm beads (right). The absence of beads between the two bottom tubes is due to the test configuration.

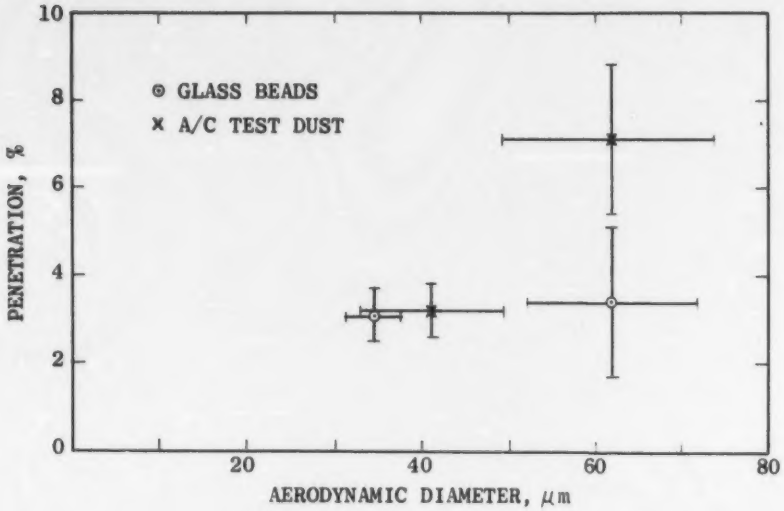

Figure 40. Penetration of the size-selective hi-vol by large glass beads and A/C test dust.

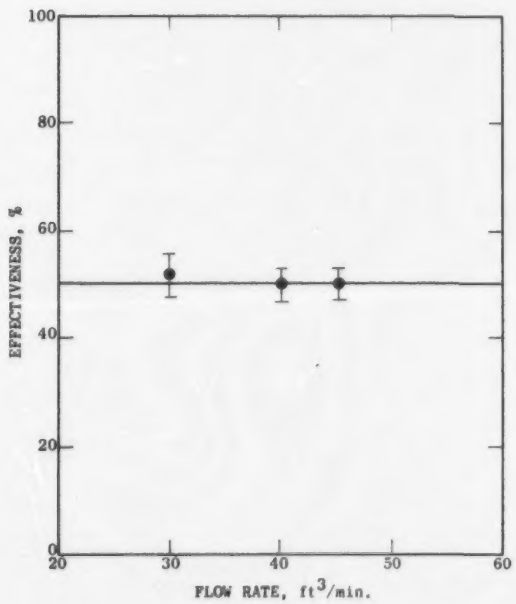

Figure 41. Sampling effectiveness of the size-selective hi-vol vs. flow rate for 15 μm DOP particles. (Data obtained by John, et al. for the California Air Resources Board, Ref. 16)

OTHER DATA ON SSI PERFORMANCE

Data on SSI performance obtained by the authors (16) under the sponsorship of the California Air Resources Board are summarized here. Figure 41 shows that the sampling effectiveness is independent of flow rate, within the errors. Table 8 lists data on the uniformity of the filter deposit. Corner-center differences are less than 5%. The coefficients of variation for corners are higher, but are related, particularly for the smaller particle diameters, to the variation in the incoming aerosol concentration. Figure 42 and Figure 43 illustrate the correlation between the concentration of the incoming aerosol at a given point on the inlet and the deposit concentration on the nearest corner of the filter. Thus an inhomogeneous aerosol cloud will produce a non-uniform filter deposit. It is conceivable that such a situation could be encountered in the field, but it seems unlikely to be a significant problem.

Large Ambient Particle Penetration

In order to evaluate the SSI performance under ambient sampling conditions, measurements of large particle penetration efficiency were made for wind-blown soil particles. The sampling site was a 5 acre newly-cleared field of dry, homogeneous and uncompacted soil consisting of finely-divided aluminum-silicate minerals. The SSI was positioned near the center of the field, upwind of the AIHL mobile laboratory which provided electrical power. For each measurement the sampler was exposed to a highly concentrated cloud of soil aerosol over a short period of time (< 10 min) to provide a worst case test of sampler performance. Highly concentrated aerosol clouds were generated on demand by the tires of a motor vehicle traversing the field approximately 20 meters upwind and allowed to drift over the sampler at the prevailing wind speed (10-20 Km/Hr).

The sampling configuration used for penetration measurements is shown in Figure 44. The aerosol concentration entering the sampler inlet was measured using 25 mm filter samplers mounted 3 cm inside the entrance slit facing the incoming air flow. Four such prefilters located 90° apart were operated at an isokinetic flow rate. Since the prefilters sampled only the aerosol entering the inlet, the sensitivity of the penetration measurements to ambient air currents was minimized. A sample of the aerosol which penetrated the inlet was collected by a 47 mm after filter. The after filter sampler was attached to the bottom of a central collection nozzle and operated at the normal nozzle flow rate (2.5 CFM). To correct for the presence of the after filter the SSI was operated at a reduced flow rate (37.5 CFM).

For both the 25 mm prefilters and 47 mm after filter, 5 μm pore size Nuclepore filters were used to facilitate particle examination by scanning electron microscopy. A standard 20 x 25 cm (8" x 10") glass fiber filter (S&S) was used on the SSI high volume sampler. Filter loadings were determined gravimetrically using a microbalance (Cahn Model 26) for the Nuclepore filters and a Sartorius semi-microbalance for the glass fiber filter. A measure of the total mass penetration was obtained by dividing the glass fiber loading by the average prefilter loading, normalized by the flow rates. In order to determine the penetration as a function of particle size, particles

TABLE 8. UNIFORMITY OF FILTER DEPOSITS IN THE SSI

Particle Dia., μm	Ave. difference, (corner-center), %	Corners σ/x, %	Entering Aerosol σ/x, %
10	- 3.2	6.0	7.9
15	- 1.5	8.7	8.8
18	- 4.9	6.0	8.5
20	- 4.0	8.9	4.7

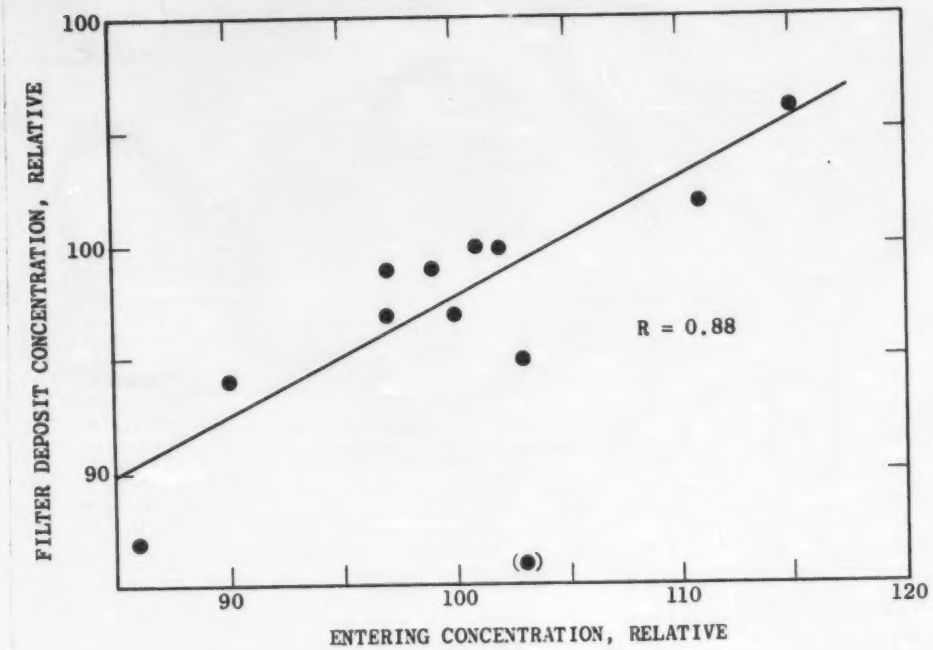

Figure 42. Correlation between the entering concentration of 10 μm aerosol particles and the filter deposit concentration on the nearest corner. The point in parentheses was omitted from the regression. (From Ref. 16)

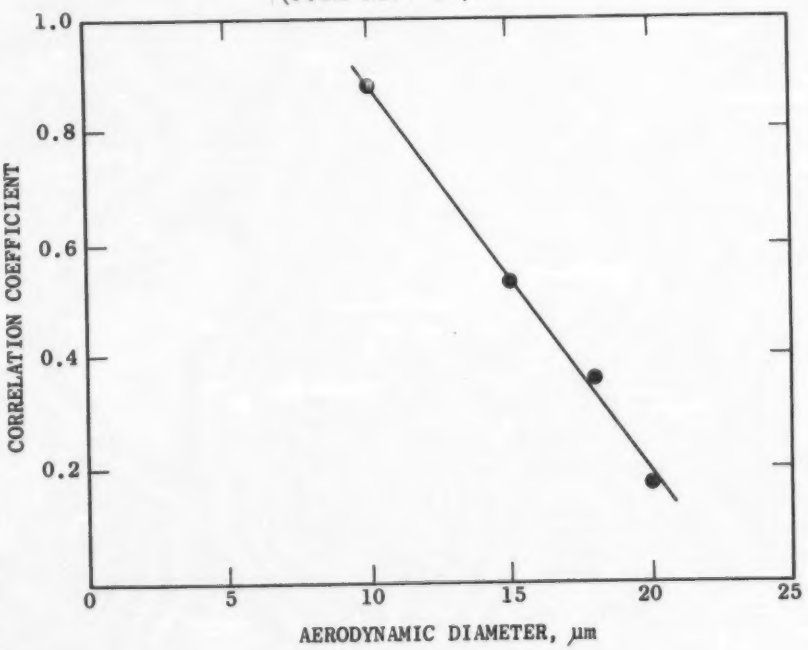

Figure 43. Plot of the correlation coefficients for various particle diameters, derived from the data as in Figure 42. (From Ref. 16)

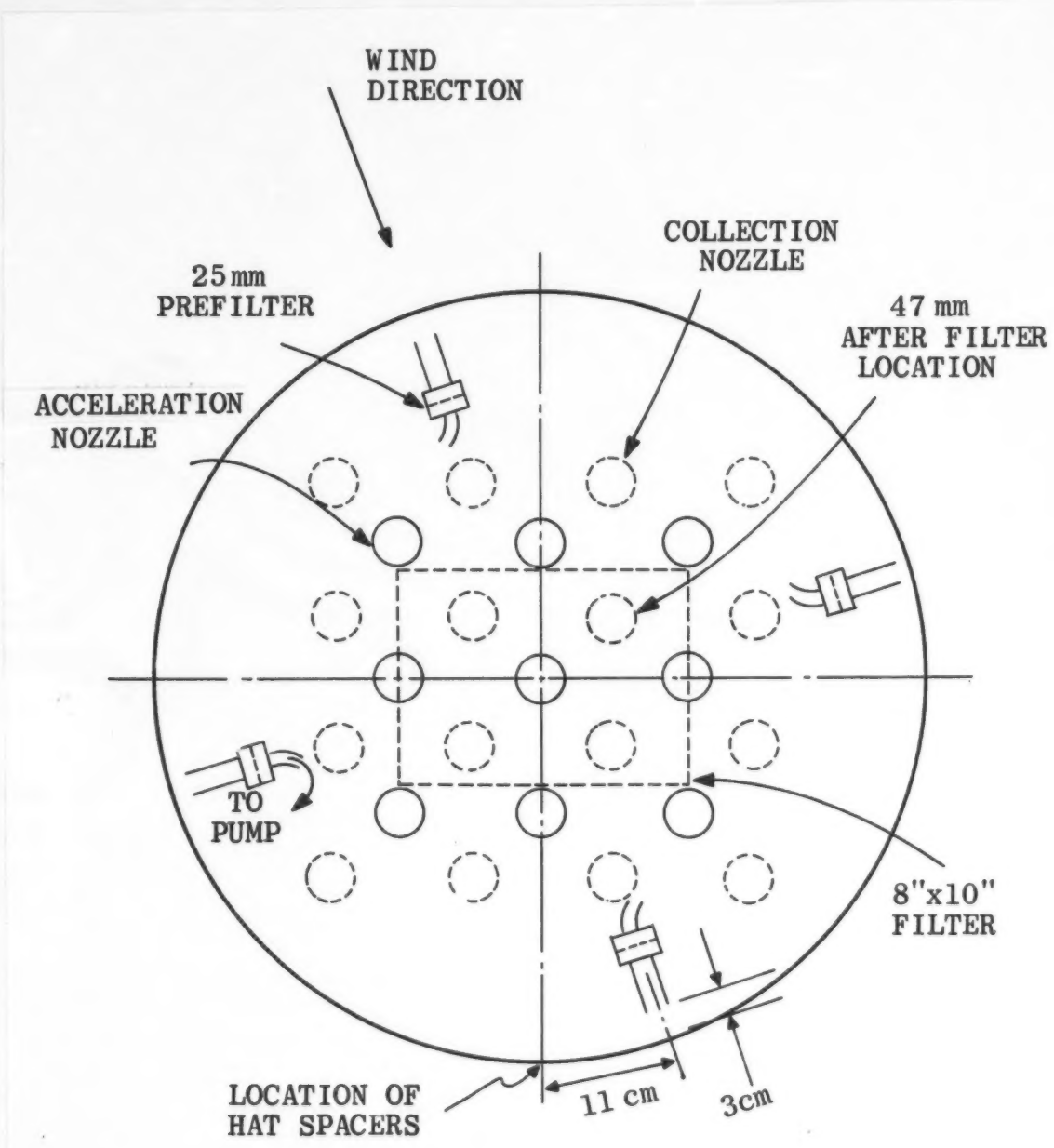

Figure 44. Arrangement for testing of the size-selective hi-vol with ambient particles.

collected on the prefilter facing into the wind and the after filter were sized on scanning electron micrographs at 660X (Figure 45a). Elemental analysis of individual particles by energy-dispersive x-ray fluorescence (Figure 45b) indicated that almost all of the aerosol was an aluminum-silicate compound (primarily Si with trace quantities of K, Ca and Fe). Particle density was determined to be near 2.7 g/cm^3 based on analysis of the bulk material by helium pycnometry. This is in agreement with values for minerals of similar composition. The size of the irregularly-shaped soil particles was calculated as the average of mutually perpendicular maximum and minimum dimensions of the particle projection in the field of view. This is a reasonable estimate of equivalent geometric diameter since most of the particles observed were approximately ellipsoidal with relatively small aspect ratios. Particle size frequency distributions for equivalent areas of the prefilter and after filter are shown in Figure 46. Particles larger than 50 μm were found to enter the SSI but no particles greater than 25 μm were observed on the after filter. Mass penetration for particles greater than a chosen diameter was calculated by multiplying the total mass penetration by the ratio of the fractional aerosol mass greater than the stated size on the after filter to that on the prefilter. The results are summarized in Table 9. A penetration efficiency of 5% for particles greater than 30 μm aerodynamic diameter is found, in good agreement with the 3-4% penetration measured for glass bead test aerosol. Also, as before, penetration increases dramatically in the vicinity of the cutpoint.

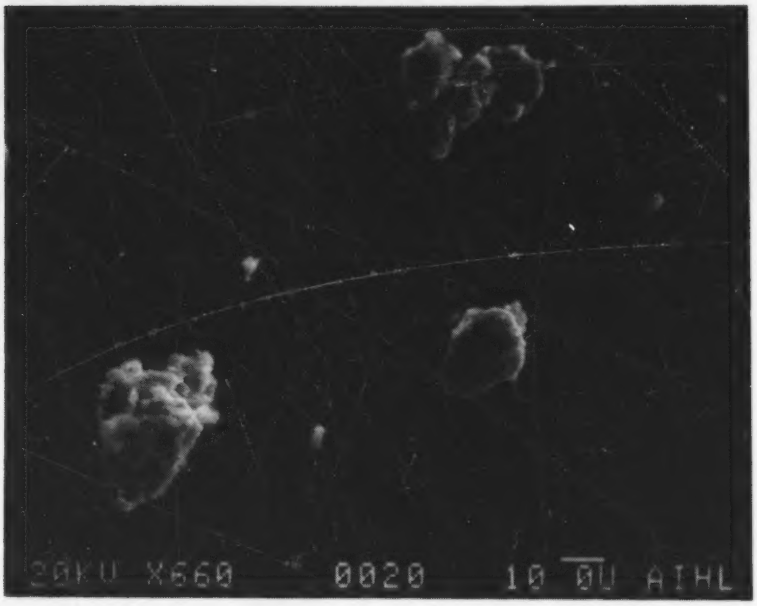

Figure 45 a. Soil particles collected on a 5μm pore size Nuclepore prefilter.

Figure 45 b. XRF spectrum of soil particles.

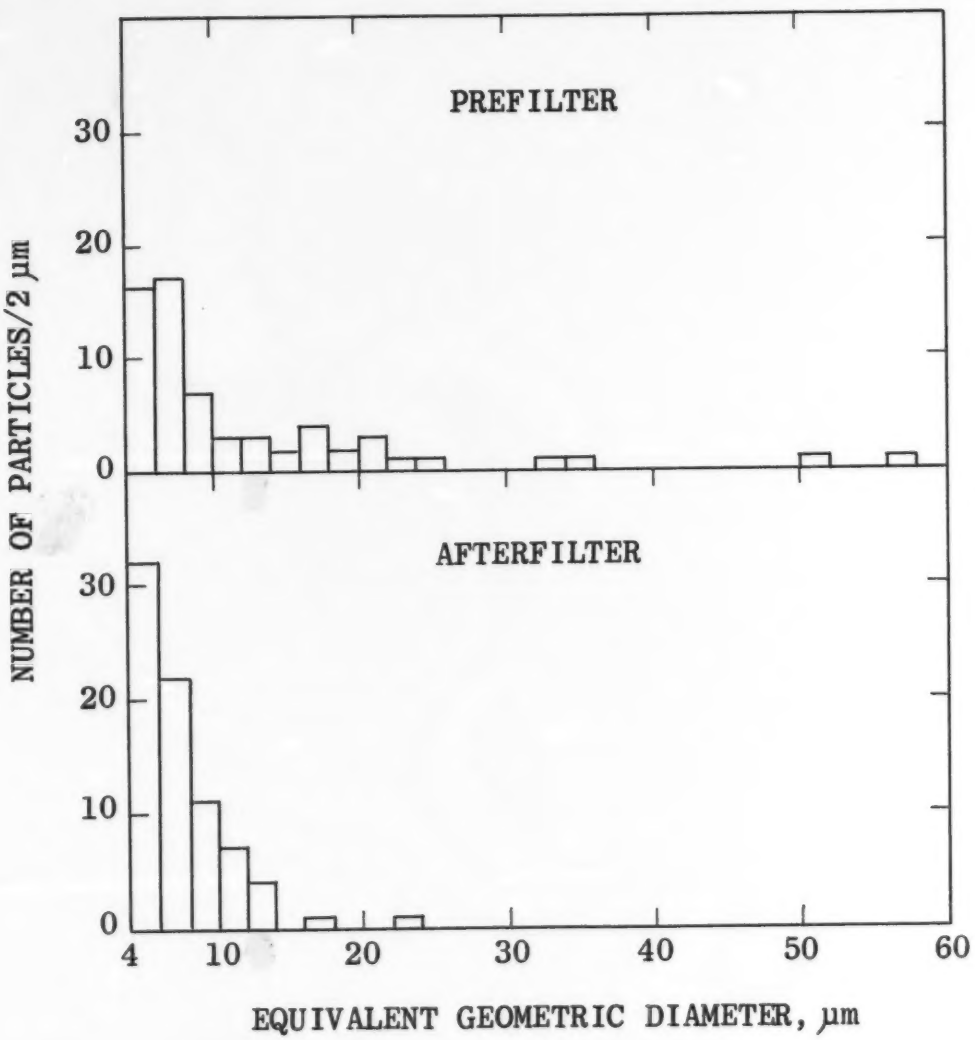

Figure 46. Size distribution of ambient particles on the prefilter and after filter inside the size-selective hi-vol.

TABLE 9. PENETRATION OF THE SIZE-SELECTIVE HI-VOL BY LARGE AMBIENT PARTICLES

$D_{geometric,}$* μm	$D_{aerodynamic,}$+ μm	Penetration, %
> 13	21	7.4
> 14	23	6.5
> 18	30	4.8

*Measured by scanning electron microscopy

+Based on a density of 2.7 g/cm^3 measured by helium pcynometry.

SECTION 7

SIDE-BY-SIDE SAMPLER TESTING IN AMBIENT AIR

Simultaneous operation of several samplers at the same outside location affords a direct comparison of their performance under "real world" conditions. The present work included duplicate samplers for determination of the variability of their results and different types of samplers for detection of any bias. The data presented here are derived from operation of a sampling array for a period of about two weeks. Because of the small sample size, the statistical accuracy of the comparison of side-by-side dichotomous samplers is limited. However, the purpose of the present effort was not to duplicate the more extensive comparisons obtained by the EPA Inhalable Particle Network but to attempt to identify physical causes of sampling errors through hands-on operation of the samplers by research personnel. In addition, the dichotomous samplers were compared to Monocut and cyclone samplers, which are not included in the EPA network.

SAMPLING FACILITY AND SAMPLER ARRAY

The ambient air sampling facility of the California Department of Health Services is located on the roof top of the eight-story laboratory building at 2151 Berkeley Way in downtown Berkeley. There are no nearby freeways and, with prevailing westerly winds, the site is generally downwind of San Francisco. From the present and past sampling, the aerosol is found to be typically urban, the fine fraction containing considerable carbonaceous material. There are few particles larger than 15 μm aerodynamic diameter.

The sampling array included two Sierra Model 244 Dichotomous Samplers equipped with the standard inlet. An AIHL cyclone (17) was operated at 22 L/min, giving a D_{50} of 2.5 μm. The cyclone was used with a 1" inlet tube covered with a simple rain hat. The cyclone supplied a fine particle sample which could be compared to the fine fractions from the dichotomous samplers. Two Sierra Monocut Samplers were also operated during the last five runs. These consist of the standard dichotomous inlet, but the inlet tube leads directly to a filter holder similar to that of the Sierra dichotomous sampler. The Monocut samplers supplied an inhalable particle sample (< 15 μm) which could be compared to the sum of the fine and coarse fractions of the dichotomous samplers.

SAMPLING PROCEDURE

The samplers were operated for 24-hour periods. Before each run the sampler flow rates were set by attaching a rotameter to the inlet tube. The rotameter was previously calibrated against AIHL standard meters. The sampler was not turned off after calibration in order to avoid hysteresis in the flow controller.

The filter medium was Ghia 2 μm pore size Teflon membrane mounted on polypropylene rings. Dichotomous and Monocut filters were 37 mm dia.; the cyclone after filter was 47 mm dia. Weighings were made on a Cahn 26 electrobalance with 0.1 μg readout. Filters were charge-neutralized by passing them between two Po-210 strips mounted on a U-shaped frame to irradiate both sides of the filter with the filter deposit on the top side.

RESULTS

Precision of the Dichotomous Sampler

Coefficients of variation derived from the data of the two dichotomous samplers are plotted in Figures 47 -- 49, for the coarse, fine and total particle concentrations. The data are fitted to the function:

$$Y = \frac{a}{x} + b$$

where Y is the coefficient of variation ($\sigma/\bar{x}$), x the mean mass concentration and a and b are constants. In all three cases b is less than 3%. Therefore a is essentially 100 σ where σ is the standard deviation; moreover σ is independent of x. This is verified by direct examination of the data and by comparison of a (see Figures 47 -- 49) to the computed mean value of σ (Table 10). Thus the performance of the dichotomous samplers is characterized by the standard deviation, independent of the particle concentration. Similar results have been obtained by Shaw, et al. (19).

It is noteworthy that the standard deviation of the coarse fraction is more than twice that of the fine fraction. Frequently workers in the aerosol field have suspected the loss of large particles from filters during handling (18), but no definitive study is available. The fact that the standard deviation of the Monocut data is close to that of the dichotomous fine fraction suggests the possibility that the presence of the fine, sticky particles inhibits the loss of the non-sticky coarse particles. On the other hand, the standard deviation of the total mass is nearly equal to the sum of the standard deviations of the fine and coarse fractions. This reflects the fact that the fine and coarse fractions of one sampler tended to vary in the same direction relative to the values from the other sampler. The loss of coarse particles alone cannot explain this.

Since the volume of air sampled was 24 m^3, the standard deviations can be expressed as a (hypothetical) error in mass of 20 μg for the fine fraction and 52 μg for the coarse fraction. However, from repeated weighings the reproducibility is within about ± 3 μg. Also since a relative comparison is

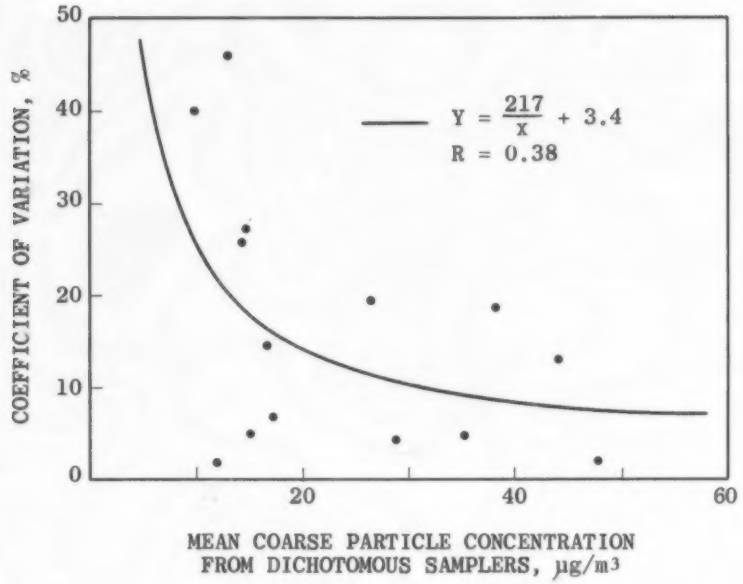

Figure 47. Coefficient of variation vs. mean particle concentration for the coarse fractions of two dichotomous samplers operated side-by-side.

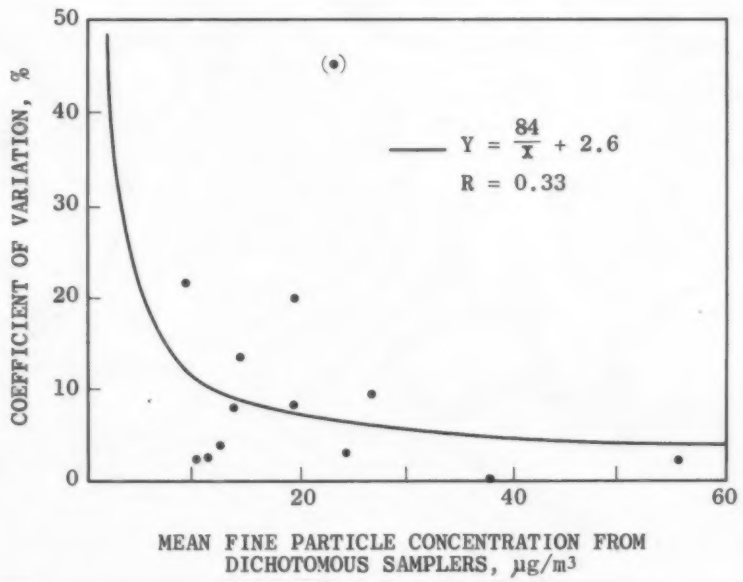

Figure 48. Coefficient of variation vs. mean particle concentration for the fine fractions of two dichotomous samplers operated side-by-side.

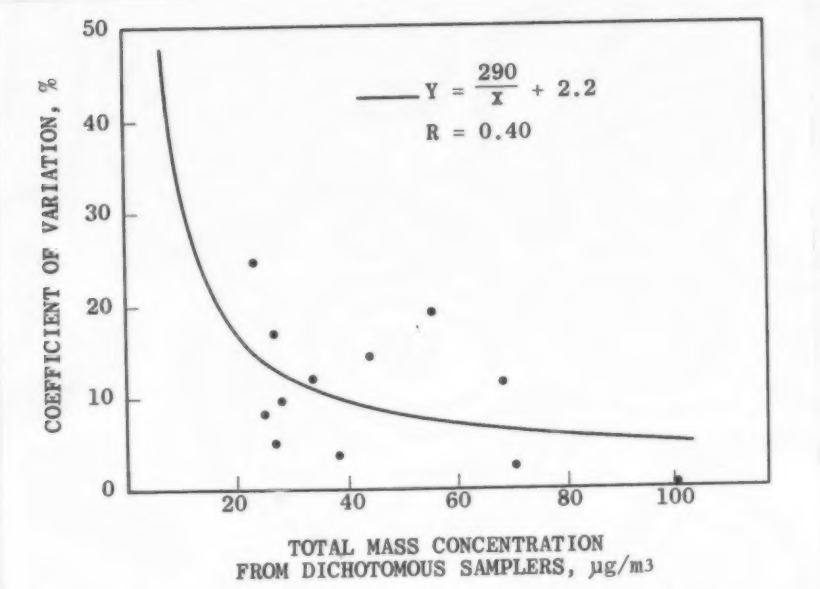

Figure 49. Coefficient of variation vs. the sum of the fine and coarse particle concentrations from two dichotomous samplers operated side-by-side.

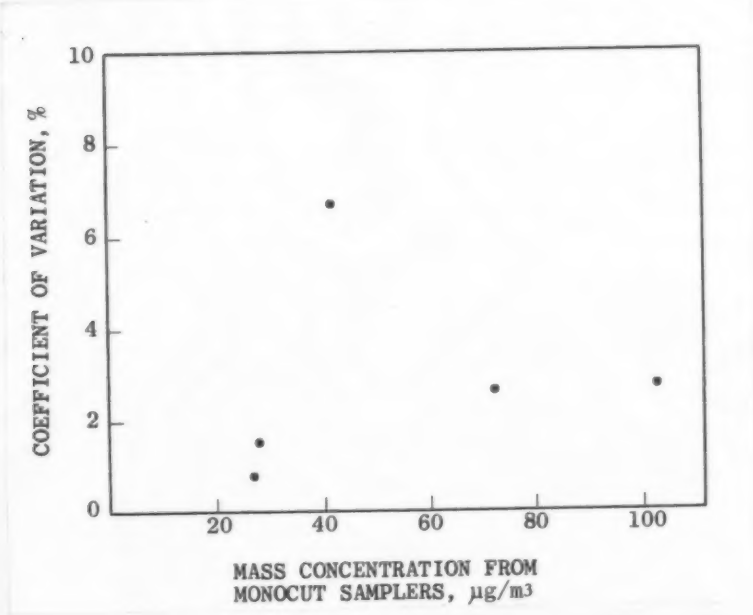

Figure 50. Coefficient of variation vs. mass concentration for two Monocut samplers operated side-by-side.

TABLE 10. STANDARD DEVIATIONS AND RATIOS OF AMBIENT PARTICLE CONCENTRATIONS FROM SIMULATANEOUS OPERATION OF SIDE-BY-SIDE SAMPLERS (Two Dichotomous samplers, two Monocut samplers and one AIHL Cyclone)

Mean Standard Deviation or Ratio			Number of Samples
$\sigma_{\text{Dichot. coarse}}$	=	2.8 $\mu g/m^3$	12
$\sigma_{\text{Dichot. Fine}}$	=	1.3 $\mu g/m^3$	12
$\sigma_{\text{Dichot. Total}}$	=	3.8 $\mu g/m^3$	12
σ_{Monocut}	=	1.6 $\mu g/m^3$	5
$\frac{\text{(Dichot. B) coarse}}{\text{(Dichot. A) coarse}}$	=	1.19 ± 0.16	12
$\frac{\text{(Dichot. B) fine}}{\text{(Dichot. A) fine}}$	=	1.11 ± 0.13	12
$\frac{\text{(Dichot. B) total}}{\text{(Dichot. A) total}}$	=	1.15 ± 0.13	12
$\frac{\text{Cyclone}}{(\text{Dichot. B})_{\text{fine}}}$	=	1.02 ± 0.10	12
$\frac{\text{Monocut Av.}}{(\text{Dichot. B})_{\text{total}}}$	=	0.98 ± 0.08	5
$\frac{\text{Cyclone}}{(\text{Dichot. A})_{\text{fine}}}$	=	1.13 ± 0.11	12
$\frac{\text{Monocut Av.}}{(\text{Dichot. A})_{\text{total}}}$	=	1.06 ± 0.06	5

being made between two samples processed under the same conditions, most of the errors cancel out. Thus effects of humidity loss of volatile components, etc., would be absent in first order.

Limited data on the coefficient of variation from two Monocut samplers is shown in Figure 50. The mean standard deviation (Table 10) of the Monocut results is about the same as that of the Dichotomous fine but much less than that of the Dichotomous coarse. Perhaps the fine (sticky) aerosol on the Monocut filter reduces the loss of coarse particles during handling of the filters.

Ratios of Concentrations from Different Samplers

Concentration ratios from different samplers are tabulated in Table 10. The fine fraction from Dichotomous sampler B agrees with the cyclone within 2% and the total from Dichotomous sampler B agrees with the Monocuts within 2%. However Dichotomous sampler A is low with respect to Dichotomous sampler B, the cyclone and the Monocuts by about 10%:

Dichot A Fine $<$ Dichot B Fine $\cong$ Cyclone

Dichot A Total $<$ Dichot B Total $\cong$ Monocut A or B

After the first six runs the flow controllers for Dichotomous samplers A and B were interchanged. However, sampler A continued to average about 10% lower concentrations. This rules out the flow controller as the cause of the bias. Sampler A was previously thoroughly validated in the laboratory (see Section 4). We have been unable to identify the reason for the bias. There remains the possibility that the location of Sampler A somehow led to lower concentrations, for example from shading by other samplers. However, the Monocuts were paired with the Dichotomous samplers and showed no bias. The location effect, if any, could be investigated by interchanging the samplers periodically during future work.

Total mass concentrations from the Dichotomous samplers correlated well with those from the Monocut samplers (Figure 51), the correlation coefficient being 1.00. The fine fraction correlated well with the cyclone data (Figure 52), the correlation coefficient being 0.99. The latter comparison is significant since two different fractionating devices are shown to agree.

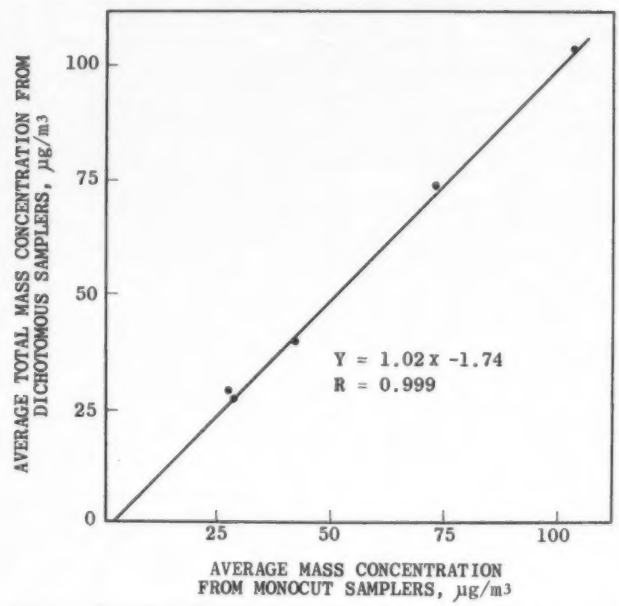

Figure 51. Correlation between the mass concentration from two Monocut samplers and the sum of the fine and coarse particle concentrations from two dichotomous samplers.

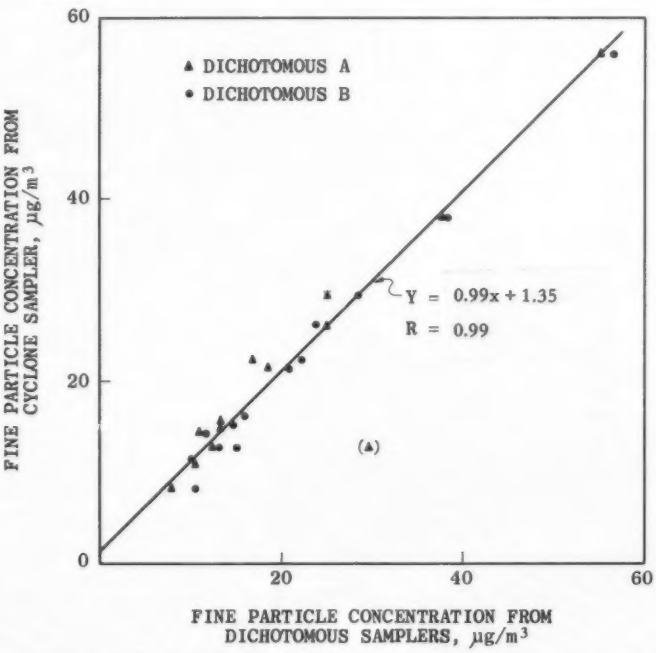

Figure 52. Correlation between the fine particle concentration from the dichotomous samplers and the AIHL cyclone.

REFERENCES

1. Miller, F. J., D. E. Gardner, J. A. Graham, R. E. Lee, Jr., W. E. Wilson and J. D. Bachman. Size Considerations for Establishing a Standard for Inhalable Particles. J. Air Poll. Control Assoc. 29:610-615, 1979.

2. Suggs, J. C., C. E. Rodes, E. G. Evans and R. Baumgardner. Inhalable Particulate Network, Annual Report: Operation and Data Summary, April 1979-June 1980. EPA-600/4-81-037, U.S. Environmental Protection Agency, Research Triangle Park, NC 27711.

3. Wedding, J. B., M. Weigand, W. John and S. Wall. Sampling Effectiveness of the Inlet to the Dichotomous Sampler. Environ. Sci. Technol. 14:1367-1370, 1980.

4. Ranade, M. B. and E. R. Kashdan. Critical Parameters for the Federal Reference Method for the Inhalable Particle Standard. Final Report, Contract No. 68-02-2725, Research Triangle Institute, Research Triangle Park, NC 27709, September 1979.

5. Berglund, R. N. and B. Y. H. Liu. Generation of Monodisperse Aerosol Standards. Environ. Sci. Technol. 7:147-153 (1973).

6. Dzubay, T. G., R. K. Stevens and C. M. Peterson. In: X-ray Fluorescence Analysis of Environmental Samples, T. G. Dzubay, ed., Ann Arbor Science, Ann Arbor, 1977. p. 95.

7. Loo, B. W., J. M. Jaklevic and F. S. Goulding. In: Fine Particles, B. Y. H. Liu, ed., Academic Press, New York, 1976. p. 311.

8. Loo, B. W., R. S. Adachi, C. P. Cork, F. S. Goulding, J. M. Jaklevic, D. A. Landis and W. L. Searles. A Second Generation Dichotomous Sampler for Large-Scale Monitoring of Airborne Particulate Matter. LBL-8725, Lawrence Berkeley Laboratory, Berkeley, California, January 1979.

9. Loo, B. W. Unpublished progress report to C. E. Rodes.

10. McFarland, A. Unpublished progress report to C. E. Rodes.

11. Wedding, J. B., A. R. McFarland and J. E. Cermak. Environ. Sci. Technol. 11:387-390, 1979.

12. Reischl, G. P. and W. John. Staub-Reinhalt. Luft 38:55, 1978.

13. McKenzie, R. L., D. S. Bright and R. A. Fletcher. Development and Characterization of a Portable Inhalable and Respirable Ambient Particulate Sampler. Unpublished Report, National Bureau of Standards, Washington, D.C., 1981.

14. McFarland, A. R. and C. A. Ortiz. Progress Report -- Aerosol Characterization of Ambient Particulate Samplers Used in Experimental Monitoring Studies. Texas A & M University Research Foundation, College Station, Texas, October 1979.

15. Wedding, J. B. Unpublished progress report, Colorado State University, Ft. Collins, Colorado, 1981.

16. John, W., S. M. Wall and J. J. Wesolowski. Size-Selective Samplers for Particulate Monitoring in California. Final Report, ARB Interagency Agreement A9-116-30, Air and Industrial Hygiene Laboratory, California Department of Health Services, Berkeley, California, October 1981.

17. W. John and G. Reischl. J. Air Pollut. Contr. Assoc. 30:872, 1980.

18. Ragaini, R. C., H. R. Ralston, D. Garvis and R. Kaifer. Instrumental Neutron Activation Analysis Techniques for Measuring Trace Elements in California Aerosols. In: The Character and Origins of Smog Aerosols, G. M. Hidy, P. K. Mueller, D. Grosjean, B. R. Appel and J. J. Wesolowski, eds. John Wiley & Sons, 1980, p. 193.

19. Shaw, R. W., R. K. Stevens, C. W. Lewis and J. H. Chance. Comparison of Aerosol Sampler Inlets. Proceedings Air Poll. Control Assoc., paper 81-5.3, Philadelphia, June 1981.